REVIEW ARTICLE

Cytometry PART A
Journal of the International Society for Advancement of Cytometry

Microfluidic Impedance-Based Flow Cytometry

Karen C. Cheung,[1]* Marco Di Berardino,[2] Grit Schade-Kampmann,[2] Monika Hebeisen,[2] Arkadiusz Pierzchalski,[3,4] Jozsef Bocsi,[4] Anja Mittag,[3,4] Attila Tárnok[4]

[1]Department of Electrical and Computer Engineering, University of British Columbia, Vancouver, Canada

[2]Leister Process Technologies, Axetris Division, Kaegiswil, Switzerland

[3]Translational Centre for Regenerative Medicine (TRM), University of Leipzig, Leipzig, Germany

[4]Department of Pediatric Cardiology, Cardiac Center, University of Leipzig, Leipzig, Germany

Received 28 January 2010; Revision Received 25 March 2010; Accepted 6 April 2010

Grant sponsor: German Federal Ministry of Education and Research (BMBF, PtJ-Bio); Grant number: 0313909;

*Correspondence to: Karen C. Cheung, Department of Electrical and Computer Engineering, University of British Columbia, 2332 Main Mall, Vancouver, Canada V6T 1Z4

Email: kcheung@ece.ubc.ca

Published online 21 May 2010 in Wiley InterScience (www.interscience.wiley.com)

DOI: 10.1002/cyto.a.20910

Abstract

Microfabricated flow cytometers can detect, count, and analyze cells or particles using microfluidics and electronics to give impedance-based characterization. Such systems are being developed to provide simple, low-cost, label-free, and portable solutions for cell analysis. Recent work using microfabricated systems has demonstrated the capability to analyze micro-organisms, erythrocytes, leukocytes, and animal and human cell lines. Multifrequency impedance measurements can give multiparametric, high-content data that can be used to distinguish cell types. New combinations of microfluidic sample handling design and microscale flow phenomena have been used to focus and position cells within the channel for improved sensitivity. Robust designs will enable focusing at high flowrates while reducing requirements for control over multiple sample and sheath flows. Although microfluidic impedance-based flow cytometers have not yet or may never reach the extremely high throughput of conventional flow cytometers, the advantages of portability, simplicity, and ability to analyze single cells in small populations are, nevertheless, where chip-based cytometry can make a large impact. © 2010 International Society for Advancement of Cytometry

Key terms

microfluidics; impedance characterization; label free; single cell analysis; hydrodynamic focusing; sorting

MICROFLUIDIC flow cytometers can bring many advantages to the field of flow cytometry (FCM). Compared to typical flow cytometry channel sizes, the miniaturized dimensions permit microfluidic systems to analyze single cells, to identify cellular variability in gene expression, or drug response within a cell population. Chip-based cytometers can have lower size and costs than conventional benchtop instruments, and may be portable. Today, the developmental aim for microfluidic systems is to reach the same sensitivity and capability for multiparametric analyses as delivered by conventional flow cytometers. Many efforts have been made to improve existing devices and to create new miniaturized high-end instruments. Microfluidic chips can incorporate on-chip cell preparation, cell culture, lysis, and modules for optical, electrophoretic, or genomic analysis (1). They are also suitable for analysis of cells in suspension as well as adherent cells.

Miniaturized cytometry devices will have high impact in the development of point-of-care devices in developing countries. Accurate $CD4^+$ T-cell counts are used to monitor human immunodeficiency virus (HIV)-infected patients, and various thresholds of the number of $CD4^+$ T lymphocytes per μl of whole blood are used to start antiretroviral therapy (2–5). A simple, single-purpose CD4 cell counting device, which does not require standard laboratory equipment or trained laboratory personnel, could help some of the 33 million HIV-infected people worldwide monitor the stage of infection (6–8). In this application, increased analysis throughput is a secondary concern compared to increased sensitivity and specificity. Portable, miniaturized cytometry devices may also be in high demand during outbreaks of influenza for virus typing (9–12), and are currently available for HIV, tuberculosis, or malaria

ISAC International Society for Advancement of Cytometry

screening, complete blood cell count measurements, and cell screening assays (13,14). Increased throughput will also benefit cell screening for drug discovery (15).

New and emerging technologies focus on the single-cell level to address demand for precise, high-content multiparameter analysis. In recent years, we have witnessed the development of large scale quantitative cellular research such as High-Content Screening which is promising for high-content and high-throughput analysis (16). Typical multiparametric analysis in the field of cytometry refers to the use of many different fluorescence dyes to identify and characterize cells. These labels can be used to distinguish between cell types, or to characterize the effects of drugs or identify drug targets within cells (17). Multifrequency impedance measurements could complement the multiparametric, high-content data that is used in drug screening.

Emerging label free technologies may obviate the need for tagging and would thus avoid perturbing the biological system. Technologies on the horizon include Raman spectroscopy, impedance cytometry, near infrared spectroscopy, and photoacoustic cytometry (18–23). Newly developed or modified instrumentation for optical imaging based on reflectance, two-photon, and multispectral imaging can detect and localize cellular signatures of cancer in vivo, without the use of contrast agents or extrinsic dyes (24). Impedance analysis, however, can be an interesting feature for cytometry as well. It offers the possibility for evaluation of cellular characteristics not feasible with common tags. Impedance spectra of cells could reveal cellular identity, as can be done with fluorescence spectra. Multiparametric analyses, therefore, might be possible with impedance cytometry as well. This label-free approach would protect cells from undesirable effects resulting from label preparation and will be interesting for many applications. Also, the combination with fluorescence and scattered light analyses sounds promising. On the other hand, simple cytometers, reduced in size and price, with perhaps a single dedicated analysis capability, are needed for crucial applications such as $CD4^+$ cell counting. Affordable, portable, and easy-to-use cytometers would be ideal for this purpose.

Particle counting is one important aspect of flow cytometry analysis; one of the first applications of electric analysis was particle counting in the Coulter chamber. In that method, particles passing through a small aperture are measured either through a voltage or current pulse. It is now the most widely used approach. Microfluidic Coulter counters have been developed which measure a change in impedance, conductance, or reflected radio frequency power (9).

One of the most widely used methods for high-throughput cell identification and cell sorting is fluorescence-activated cell sorting (FACS). Although the fluorescent labels permit molecular-level detection, they can be expensive, laborious, time-consuming, and inherently alter the cell: immunological tagging requires an incubation step, antigenic exposure risks triggering cell differentiation, and non-surface markers require membrane permeabilization. Conventional flow cytometry systems are not portable and require skilled operators. Microfluidic FACS systems have also been developed (25), incorporating on-chip optical elements including waveguides (13,26). Recently developed microfluidic optical systems have also used a DVD pickup head to detect beads and erythrocytes (27).

Impedance-based cell characterization extends beyond the Coulter measurement. Microfluidic impedance systems have been developed to characterize both adherent cells as well as cells suspended in a flow (28). All of these techniques are constantly improved whereby impedance analysis seems to have the best chance for miniaturized devices and the broadest range of applications.

Impedance Analysis as a Label-Free and Non-Invasive Technique

Cell characterization through dielectric properties does not require immunological markers, which can be expensive and fragile, with short shelf-life. Dielectric properties such as membrane capacitance and conductivity reflect membrane morphology and function, which in turn correlate with physiological differences between cells or pathological changes in cells over time. Changes of ion channel status in the cell membrane, intracellular ion flow into the endoplasmic reticulum and into mitochondria, as well as changes in morphology or nuclear size are all readily detected as changes in dielectric properties whereas they would not be detected using biochemical or immunological techniques. Pauly and Schwan (29) determined the dielectric properties of cells by measuring the electrical impedance of a cell suspension. The cells are modeled as a spherical cytoplasm surrounded by a thin membrane. Dielectric spectroscopy in macroscopic cell suspensions has already been used to monitor cell growth in batch populations (30). Impedance spectroscopy has also been used on-chip to analyze the intracellular components of lysed cells (31) or for chemical cytometry (32). Other previous work involving microfabricated devices has used dielectrophoretic (DEP) forces to characterize the dielectric properties of individual cells (33). The dielectric properties of cells can be inferred from the motion or levitation of the cells resulting from their polarization in a non-uniform electric field (34). Both the DEP crossover frequency and the speed of rotation (electrorotation) indicate the response of the cell to this non-uniform electric field. Gascoyne et al. (35) have discriminated cancerous and non-cancerous cells using electrorotation, which characterizes cells at the rate of several minutes per cell.

In contrast to electrorotation or the measurement of DEP crossover frequency, impedance-based flow cytometry measures the impedance of a cell in a detection volume and thus measure the dielectric properties of the cell directly. Typically, this setup features microfluidic chips in which each cell passing by an integrated detection site is measured individually in an electric field (Fig. 1) (36,37). The corresponding impedance spectrum of the control volume will depend on the dielectric properties of the cell inside. At low frequencies, the cell membrane offers significant barrier to current flow and the impedance amplitude gives the cell size. The conductivity of the detection volume depends only on the relative volume of the cell; in fact the low frequency conductivity is the impedance

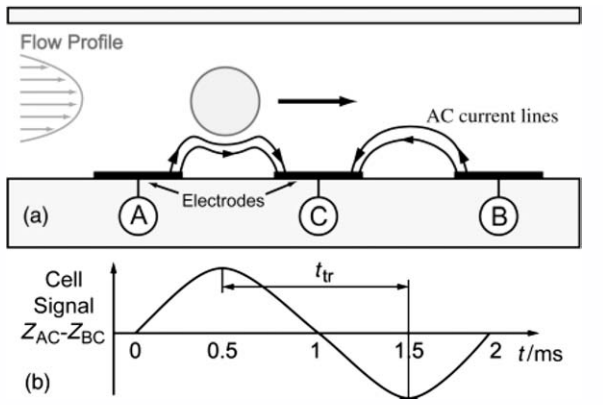

Figure 1. Side view of a microfluidic impedance flow cytometer. The cell passes over electrodes and the impedance of the detection volume is measured (Reproduced from Ref 36, with permission from Royal Society of Chemistry). Depending on the frequency, the measurement can give information about cell size, membrane, or cytoplasm properties.

parameter detected in a Coulter volume measurement (38). At intermediate frequencies, membrane polarization is reduced, and impedance measurements give information about membrane properties. At high frequencies, the membranes are minimally polarized, and measurements here give information about intracellular structures and the cell interior. Thus, analysis of the dielectric spectrum in the frequency range of 40 Hz to 1 GHz yields information on membrane capacitance, cytoplasm conductivity, and cytoplasm permittivity as a function of frequency. Opacity, the ratio of the impedance magnitude at a high frequency to a low frequency, can be used to normalize the data for both cell size and cell position between the measurement electrodes in the microfluidic channel (39). The measurements can be correlated with analytical dielectric models of the cells (shelled particle enclosing conductive interior, suspended in homogeneous conductive medium) based on Maxwell mixture equations (37,40,41). Thus, impedance-based flow cytometry has the promise to improve the sensitivity of Coulter technology.

Microfluidic flow cytometer chips have been fabricated through traditional micromachining techniques using glass or silicon substrates, or through molding, most commonly via soft lithography (42). In the soft lithography replica molding process, elastomeric polydimethylsiloxane (PDMS) structures are molded from photolithographically defined structures to define microchannels and inlet/outlet reservoirs (43). To form closed channels, the PDMS is bonded to a separate glass substrate on which thin-film electrodes are first patterned, typically using a lift-off process. The electrodes can be patterned through photolithography followed by either metal etching or liftoff, through stencil or screen printing, or through nanoimprint lithography of a UV curable resist followed by metal liftoff (28). Such chips can be inexpensive to fabricate, and when integrated with electronics and sample delivery, can comprise part of a more portable and lower-cost system compared to conventional flow cytometers.

Summary of Impedance-Based Cytometers Presently on the Market

Coulter and Hogg first described the technique for simultaneous AC (alternate current) and DC (direct current) impedance measurements in the 1960s (44) to be able to separate particles of the same size but of different composition. In the 1970s and 1980s, Hoffman and Britt demonstrated in a flow cytometry system that cells with the same Coulter DC volume could be distinguished using high frequency impedance measurements (38,45). Leif et al. developed flow cytometers which integrated Coulter measurement, high frequency impedance, and fluorescence detection (46–48). Existing impedance-based cytometry systems in the market can be grouped according to their principle of analysis: (1) surface impedance analyzers equipped with electrodes covering the surface of the measurement spot, including chip-based and multiwell-based systems (2); impedance-based flow cytometers conceived mainly for cell counting and sizing applications.

The Z series Coulter Counters belong to the group of flow cytometers which were the first impedance-based cytometers introduced in the early 1960s (38). The CASY is another analyzer based on the same principle, and was introduced by Innovatis AG (Roche). The same basis for analysis was also implemented in the Beckman Coulter Quanta system, which provides additional information on side scatter and fluorescence analyses (49). Sysmex and Abbott (such as the Cell Dyn series) also manufacture instruments which can measure impedance, particularly for platelet counting (50). To reduce error in the platelet size range, where fragmented erythrocytes and noncellular particulates can overlap, the Coulter LH 750 system incorporates data extraction and other algorithms for impedance-based platelet counting. Newer impedance flow cytometers expected on the market (in 2010) include the new Millipore Scepter, an automated hand-held instrument which resembles a pipette. This instrument is intended for counting and sizing.

The microfluidic cytometry technology highlighted in this article has some advantages compared to the systems described above. Compared with Coulter Counters (Z series, CASY), which usually measure the impedance signals using DC or low AC, microfluidic impedance flow cytometry (IFC) provides the possibility to perform impedance measurements at different frequencies covering a range of 100 kHz to 20 MHz. As already documented from various groups (18,51,52), it was shown that at such frequencies (starting from 1 MHz) other parameters (cellular membrane capacitance and cytoplasmic conductivity) can also be interrogated and provide additional information (besides number and size).

The group of impedance-based instruments which cover the field of adherent cell surface measurements include several tools presently available in the market, with examples from Bionas and ACEA Biosciences (including the Roche xCELLigence System derived from ACEA), which monitors proliferation of adherent cells (53,54). These systems were recently summarized by Xi et al. (55). Aber Instruments produces systems which monitor viable biomass, for applications including monitoring yeast in fermentation and brewery processes.

When comparing IFC with chip-based impedance spectroscopy (56–58) it is clear that both systems were made for different purposes. The first is primarily targeted for cells in suspension whereas the latter is intended mainly for adherent cells and tissues. Thus, both systems have complementary, non-overlapping applications. IFC mainly focuses on changes in individual cells, analyzing thousands of cells per sample. In contrast, chip-based impedance spectroscopy describes intercellular interactions—changes in morphology, cell-to-cell contact in general (59), and monitoring changes in cytoskeleton resulting from changes in cell contact with the chip (culture surface). This technique does not provide information at the single cell level but yields mean values for the cell population adherent on the chip (60). On-chip impedance spectroscopy also allows measurements of small tissue fragments which may become the standard for chemosensitivity of cancer tissues and drug discovery assays. Another difference between both systems is that chip-based impedance spectroscopy measurements can be used for real-time monitoring in the tissue sample or cell culture (61). IFC measurements, in contrast, provide snapshot information per cell (15). Thus, IFC is suited for end point experiments. Both systems open the opportunity to measure impedance over a spectrum of frequencies, allowing for later frequency selection. The combination of IFC with other cell analysis systems such as FCM as proposed by the group of Morgan (52) could help to understand sub-populations identified by IFC. This would allow more reliable cell characterization and would lead to enrichment of the parameter pool for cell status description. This in fact constitutes the basis for the cytomics approach to unwinding the cellular biocomplexity of organisms starting at the cellular level (62).

The functional heterogeneity of cytomes results from both the genome and external environmental influences. Cytomics can be considered as a discipline that links genomics and proteomics to cell and tissue phenotype and function, as modulated by external influences. Of special importance is the cell-by-cell basis of cytomics analysis. This approach allows the user to resolve heterogeneous systems by avoiding the loss of information that characterizes bulk technologies, where average values are obtained from large number of cells or from tissue homogenates (62). The cytomics approach reflects the reality that cells and their inter-relationship, and not genes or biomolecules, represent the elementary functional units of organisms.

This article examines recent progress in microfluidic impedance-based flow cytometry, including new approaches to focusing particles within the channel for improved reproducibility. This article also presents new data demonstrating that multiparameter impedance spectroscopy flow cytometry can be used to distinguish cell viability, changes in membrane potential, and changes in intracellular ion concentration. Such systems could be incorporated into laboratories for routine analysis.

Technological Improvements

Recent work has focused on improving the sensitivity of microfluidic impedance flow cytometry measurements. Factors which influence the sensitivity include the volume fraction of the cell, the presence of a double layer capacitance over the electrodes, and the position of the cells in the flow.

Microfluidic Coulter Systems, Sensitivity

In the low frequency limit, the cell is non-conducting due to the capacitance of the membrane, and the conductivity of the detection volume depends only on the relative volume of the cell (38): $k_o = k_s(1 - p)/(1 + p/2)$ where k_o is the conductivity of the detection volume in the low frequency limit, k_s is the conductivity of the external medium, and p = (particle volume)/(detection volume) is the volume fraction of the cell. Thus, scaling the size of the detection volume with the size of the particles (mammalian cells $\sim$10 μm; bacteria $\sim$1 μm), good signal can be obtained.

Instead of scaling the microfluidic channel, Rodriguez-Trujillo et al. (63) have used hydrodynamic focusing to define the sample flow, thus using a single device to characterize a wide range of sample particle sizes. By using low-conductivity sheath flows, Rodriguez-Trujillo et al. (64) created a virtual adjustable aperture, since the width of the sample flow could be varied from 12 to 100% of the width of the channel by varying the central flow rate. They demonstrated particle counting of 20 μm particles (1,000 particles/s) as well as yeast cells of 5 μm diameter, using co-planar microelectrodes in PDMS microchannels. The use of non-conducting sheath flows increased the sensitivity of their micro-Coulter system, since the measured resistance is mainly due to the conductivity of the sample flow. In this way, a relatively large channel (on the order of 100 μm $\times$ 43 μm) can be used even for the detection of small particles.

Wood et al. (65) used a radio frequency (RF) reflectometry measurement to achieve high-throughput detection. The tunable RF tank circuit was tuned to achieve low reflectance. The passage of a particle would change the impedance of the detection volume and increase the reflectance from the embedded electrodes. By monitoring the reflectance in the channel at frequencies as high as 100 MHz, the measurement avoided the double-layer interfacial impedances at the electrode surface, permitting high sensitivity measurements at a throughput of $\sim$5,000 beads/s. Nikolic-Jaric et al. (66) used a microwave frequency system for capacitive detection of microspheres and cells.

Jagtiani et al. (67,68) fabricated several apertures in parallel to increase the throughput of Coulter counting. The four-channel device had a common electrode and common sample reservoir. All of these devices were meant for counting and possibly sizing purposes. Only with the possibility to vary the impedance measurement frequency, however, was it demonstrated that the microfluidic approach has the potential for cell characterization (18,51,69–71).

Electrode polarization can be problematic for impedance characterization. A double-layer capacitance forms over metal-based electrodes, which dominates the signal at DC and at low frequencies, reducing the capability to study effects on the cell membrane or the α-dispersion. Previous work has used low-conductivity suspending media containing sucrose or dextrose

(33) to reduce this polarization effect. Low-frequency or DC input can also cause Faradaic reactions at metal electrodes, causing them to erode. Chun et al. have developed salt-bridge based electrodes (72) to improve the sensitivity of particle sizing. The salt bridges fabricated by Chun et al. consisted of microfluidic channels filled with NaCl solution, into which Ag/AgCl electrodes were immersed. This setup permitted DC impedance analysis of beads as well as red and white blood cells (WBCs) at a rate of 1,000/s. Another advantage of the salt bridge electrode is velocity-independent signal amplitude even at the speed of 100 mm/s. The polyelectrolyte gel electrodes were used to measure DC impedance signals to count red blood cells (RBCs) in diluted whole blood (73). This DC impedance cytometer using polyelectrolyte gel electrodes has also been integrated with light emitting diodes (LEDs) and solid-state photomultipliers to build a portable system for simultaneous fluorescence and impedance detection (74). Demierre et al. also used a setup in which large electrodes are placed distant from the microfluidic channel to create non-uniform electric fields for dielectrophoretic particle manipulation (75). By avoiding electrode polarization using these electrolyte-based electrodes, impedance flow cytometry may be applied at very low frequencies to examine ligand binding or other cell membrane events.

Single Cell Dielectric Spectroscopy: Multifrequency Analysis

In contrast to measurements of single cells at discrete frequencies, Morgan et al. have developed a method for broad band multifrequency analysis of cells using pseudorandom signal generated by a maximum length sequence (MLS) system (76–80). This method permits the characterization of cells within 1 ms at 512 discrete frequencies ranging from 976 Hz to 500 kHz.

Multifrequency analysis could allow the user to distinguish cell types from one another based on cell size, cell membrane properties, intracellular properties, or a combination of these factors. A mixture of cells could be sorted into subpopulations. Alternatively, a single population of cells could be sorted for response to an external agent and effect on viability, membrane polarization, or other factors. By extending the measurement to extremely low frequencies [within the range of the α-dispersion (81)], impedance spectroscopy may even permit analysis of ligand binding events on the cell membrane. This would be a powerful tool for drug discovery (82). Multifrequency and multiparametric analysis are further discussed below.

Particle Positioning

In conventional flow cytometers, particle focusing is achieved using coaxial flows. In optical flow cytometers, particle position within an optical detection beam should also be consistent, since laser beams typically have a Gaussian intensity profile so that a particle at the edge of the beam may give less fluorescence intensity than a particle in the center of the beam. Likewise, in microfluidic impedance-based flow cytometers, consistent particle position is a crucial factor for reproducible impedance measurement. The electrodes are typically either channels with single-sided (co-planar) electrodes embedded on one side of the channel, or channels with electrodes embedded in facing sides (parallel electrodes). In both cases, the sensitivity of the impedance measurement is dependent on the position of the particle (36,83). It has been shown that the facing electrode design provides a more homogenous electric field, which is more tolerant to the position of the particle in the microfluidic channel (39,83) and thus might not require, for some applications, the need of a focusing functionality.

Microfluidic systems for particle positioning have been developed which use microscale hydrodynamic effects (84) or external forces applied using a magnetic or electric field [electrophoresis and dielectrophoresis (33)]. Several of these approaches are reviewed below.

Particle positioning: Hydrodynamic focusing. Hydrodynamic focusing through sheath flows can be used to position a particle within the flow. Sheath flows will align the particles into a narrow stream within a wider channel. The width of the focused sample flow should be comparable to the particle diameter to ensure that the particles move one by one through the detection area—a wider core flow may permit the particles to overlap. Although a narrow channel would obviate the need for focusing, a smaller channel diameter would increase the risk of clogging as well as the back pressure and shear stress.

Lateral flow focusing has been found to reduce the signal variance (85). Lateral sheath flows are easily created using the same photolithography step which defines the sample flow. Focusing the particles in both the lateral as well as vertical dimensions could further decrease variance. Vertical focusing can also be achieved when the height of the sheath flow is greater than the height of the sample injection flow, but this approach can involve complex microfabrication steps compared to the single-layer microfluidic systems used in simple lateral flow. Simonnet et al. (86) used channels of three different depths as well as four inlets to create both vertical and lateral focusing in a high-throughput device which could analyze up to 17,000 particles/s. This involved three lithography steps and two different formulations of the UV-curable SU-8 epoxy to create the PDMS mold master with three-level relief.

Wolff et al. introduced a "chimney" to provide focusing in the vertical direction (26). The sample inlet was etched vertically through the substrate to provide a coaxial flow with the buffer. This "chimney" focusing was also used to provide a vertical focusing flow in the work of Rodriguez-Trujillo et al. (63), in which an orifice was drilled perpendicularly through the substrate to provide vertical focusing in addition to the lateral flows. Through this method, the detection sensitivity was increased by a factor of 1.6 when compared to simple lateral focusing conditions.

In contrast, Kummrow et al. (87) developed an ultraprecision micromachining process to facilitate vertical as well as lateral focusing. An aluminum or brass mold insert was milled and then used for hot embossing into polymethyl methacry-

late (PMMA) or polycarbonate (PC) plates. The milling process provides the capability to fabricate a mold which defines several channel heights.

Tsai et al. (88,89) combined lateral sheath focusing with vertical focusing, using a weir structure to separate particles directly over the detection area.

One drawback of using sheath flows is dilution of the sample. Golden et al. (90) used chevron-shaped groove features on the microfluidic channel surfaces to generate vertical sheathing after first using lateral sheath flows. The grooves can be used to ensheath a flow, and then due to Stokes reversibility, a subsequent mirror pattern of grooves can be used to separate the sample and sheath fluids (91). Choi et al. (92) used slanted obstacles in the flow channel to focus Jurkat cells to the channel centerline with 1.7% CV at a flowrate of 4 μl/min. This hydrophoretic focusing does not require accurate flow control or calibration of sheath flows.

Kim et al. (93) superimposed electrophoresis and pressure-driven flow to achieve sheathless three-dimensional focusing of RBCs. In this approach, the electrophoresis was used to drive the RBCs in the opposite direction of the fluid flow. As particles which lag behind the Poiseuille flow will migrate toward the channel axis, the RBCs were able to be focused to a position within three cell diameters of the channel centerline. Although this work demonstrated that non-spherical particles could be thus focused, the particles must be electrically charged in this approach.

Particle positioning: Inertial flows. More recently, inertial effects within the flow have been used to separate as well as focus particles within a stream. Size-based particle separation can be achieved by designing the channel geometry to induce differential inertial lift and viscous drag forces on the particles. In cylindrical channels, neutrally buoyant particles have been found to accumulate at an equilibrium position at ~0.6 tube radii from the axis, irrespective of their initial position (94). In a rectangular duct, particles migrate to a location near a corner or at the centre of an edge (95). As the Reynolds number *Re* increases, inertial forces become significant and particles can migrate across fluid streamlines and concentrate at precise equilibrium positions in the cross-section of the channel. Even within microfluidic devices, this effect produces continuous, ordered streams of particles in precise positions at high flow rates. At high Reynolds numbers, two dominant inertial lift forces act on particles: a "wall effect" which tends to force particles away from the wall of the channel, and a shear-gradient-induced lift force that directs particles toward the wall (96). These two forces are balanced at the equilibrium position of the particle, away from the channel center (97). Stokes drag ($F_S = 3\pi\mu RU$) balances the inertial lift force, while the transverse migration velocity away from the channel centerline scales as R^3, so that it is possible to separate particles of different size (R) based on their differential migration.

Curved microchannels have been used to apply centrifugal inertial forces to particles in a fluid and alter their position in the channel (Fig. 2a) (98,99). Curved channels can induce secondary rotational flow (Dean flow) caused by the inertia of the fluid. The Dean number (De) is given by: $De = \frac{\rho U_f D_h}{\mu}\sqrt{\frac{D_h}{2R}} = Re\sqrt{\frac{D_h}{2R}}$, where ρ is the density of the fluid, U_f is the average fluid velocity, μ is the fluid viscosity, R is the radius of curvature of the channel path, Re is the channel Reynolds number, and D_h ($D_h = 2wh/(w+h)$) is the hydraulic diameter of the channel. For $De < 50$, the Dean flow is characterized by two counter-rotating vortices (Fig. 2b), where flow is directed outward at the channel midline and inwards at the edges of the channel. The De increases with higher channel curvature (smaller R), larger channel diameter (larger D_h), or faster flows (higher Re). There are no dean flows in straight channels ($De = 0$). Inertial lift and Dean drag forces balance to determine the equilibrium position of particles in a curved channel. The Dean vortices reduces the number of equilibrium positions from 4 in a straight rectangular channel to 1 (near the inner microchannel wall) in a curved channel for $2R/D_h > 0.1$ (Fig. 2c) (95). Smaller particles (smaller R/D_h for a given channel) will continue to recirculate along the Dean vortices due to higher viscous drag. Preferential focusing dominates for particles with $R/D_h \sim 0.1$. Precise ordering of initially scattered particles can be observed longitudinally along the direction of flow as well as laterally across the channel. For bacteria with diameter ~1 μm, the flow focusing channel should have $D_h < 14$ μm, which is easily achievable using soft lithography microfabrication techniques. Spiral microchannels have been used to both focus larger ~10 μm particles in a single stream as well as concentrate smaller 1–2 μm particles to the outer half of a channel cross section (100). In this way, sample preconcentration and particle positioning could be achieved at $De \sim 0.47$ ($Re \sim 5$). High-throughput separation and filtration of 1 ml/min has been achieved for rigid particles, deformable emulsions, and platelets from whole blood using inertial focusing in asymmetrically curved microchannels (101).

Mao et al. (102) have also used Dean flows to demonstrate particle focusing using 7.32-μm and 8.32-μm diameter polystyrene beads of 1.05×10^3 kg/m^3 density. These particle properties are similar to those of human CD4$^+$ T lymphocytes (diameter: 8.5 μm, density: 1.07×10^3 kg/m^3). The maximum flow velocity used in their work was 3.6 m/s, within the range of normal flow cytometry devices, and they conclude that the shear rates would not damage cells during focusing. They achieved coefficients of variation (CV) of 9–15%. Lee et al. (103) used an array of contractions and expansions in a single-layer device to sheath and focus a flow of RBCs in three dimensions using only one sheath inlet. The contractions cause a secondary rotating flow, and the sheath flow wraps the sample flow.

This technique can be operated in continuous flow mode for continuous separation and pre-concentration of microparticles in a large sample volume. Hur et al. used 250 high aspect ratio channels in parallel with sheathless inertial cell focusing to demonstrate image-based RBC and leukocyte cell counts at a sample rate of up to 10^6 cells/s (104). Particles can be focused to streams of widths equal to the diameters of the particles, at channels Reynolds number up to 270 (105). The use of inertial effects to separate and focus the cells into a single

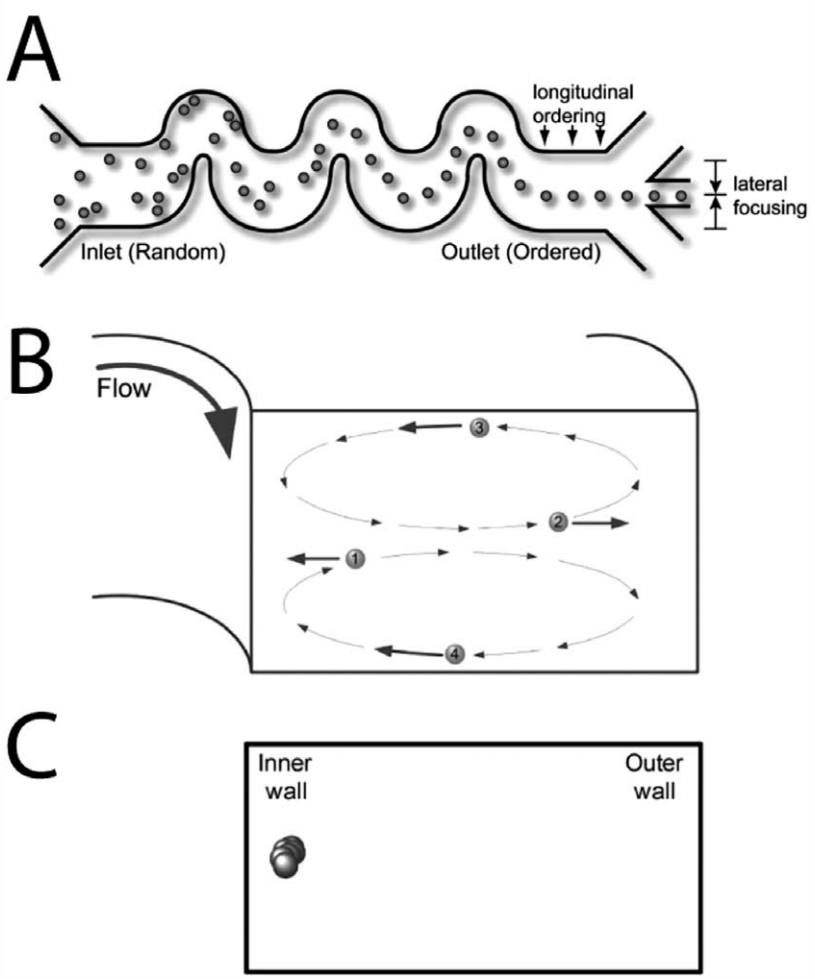

Figure 2. Inertial effects can be used to position particles in microfluidic channels. **A**: Precise inertial self-ordering of particles in a curved channel (Reproduced from Ref 98, with permission from Copyright 2007 National Academy of Sciences). **B**: Cross-sectional view showing Dean vortices and (**C**) single equilibrium position (Reproduced from Ref 100, with permission from The Royal Society of Chemistry).

equilibrium position thus is one promising approach to simplify the dielectric characterization, by preconcentrating as well as focusing the cells into a single well-defined position in the measurement channel.

Particle positioning: Dielectrophoretic forces. DEP forces scale as $F_{DEP} \sim R^3$ where R is the size of the particle, and thus may not be sufficiently effective at high flow rates to capture small particles from the flow when hydrodynamic forces are high, at high flow velocities. Therefore, these methods are typically operated in batch mode (106), a disadvantage when an application requires the extraction of particles from large sample volumes in a short amount of time. The DEP force is also a function of the fluid suspension, and liquids of different conductivities may be required depending on the particles. The DEP force also decays quickly with distance from the electrodes, so that in large channels, regions far from the electrodes will not be affected by the DEP force. This requires that the channel dimensions be scaled to the size of the particles to be manipulated. Recent work has used DEP forces trap bacteria from a continuous-flow sample stream at 100 μl/h (107), and combined DEP forces with hydrodynamic focusing to fractionate yeast cells (108).

In contrast to previous approaches involving AC dielectrophoretic focusing, Zhu et al. (109) demonstrated DC electrokinetic focusing using a serpentine channel. In this geometry, the particles experience a negative dielectrophoretic force which deflects the particles toward the channel center region. The electric field of ~20 kV/m drops across the entire length of the channel, and the authors estimate that particles can be focused at a rate of 1,200/min.

A summary of recent progress in particle positioning using microscale flow phenomena is presented in Table 1.

Impedance-Based Flow Cytometry—New Applications

Recently, microfluidic impedance cytometers have been used to analyze a wide variety of particles, including animal

Table 1. Recent progress in microfluidic focusing

PARTICLES ANALYZED	FOCUSING METHOD	DEMONSTRATED DETECTION RATE OR MEAN FLOW RATE/SPEED	REFS.
Microspheres	Ultraprecision micromachining for hot embossing in PMMA or PC	Up to 3 m/s or 20 μl/min	(87)
Microspheres	Sheath flow with micro-weir structures	–	(88)
Microspheres	DC electrokinetic focusing in a serpentine channel	1,200/min	(109)
Microspheres	Dean flows	3.6 m/s	(102)
Microspheres; *S. cerevisiae* yeast	Vertical focusing inlet	1,000/s	(63)
Microspheres; *S. cerevisiae* yeast	Vertical and lateral hydrodynamic focusing in three-level PDMS channel	17,000/s	(86)
Microspheres; *E. coli*	Sheath focusing with chevron-shaped grooves on channel surface	Total flowrate 210 μl/min	(90)
Erythrocytes	Sheathless focusing—superposition of electrophoresis and pressure-driven flow	$\approx$1.77 mm/s	(93)
Erythrocytes	Secondary rotating flow—array of contractions and expansions in single-layer device and one sheath inlet	Total flowrate 4.1 ml/h	(103)
Dilute whole blood: erythrocytes and leukocyte counts	Sheathless inertial focusing—256 high aspect ratio parallel channels	Total flowrate between 5.5 μl/min and 2.5 ml/min; up to 10^6 cells/s	(104)
Jurkat cells	Sheathless focusing—slanted obstacles in flow channel	4 μl/min	(92)

and human cell lines (51), pollen (67), phytoplankton (69), erythrocytes (18,71), and immuno-labeled beads (70). Holmes and Morgan have also used antibody conjugated beads as impedance labels to identify the CD4 T-lymphocyte population within whole blood using a microfluidic impedance cytometer (110). A summary of recent progress in microfluidic impedance-based flow cytometry is presented in Table 2.

In this review article we present a multitude of examples of application of microfluidic impedance cytometers which cover eukaryotic cell lines including cell viability and cell physiology measurements, blood cells phenotyping, and micro-organism cell viability assays. All experiments were performed on a microfluidic IFC prototype from Leister Process Technologies, Axetris Division (Kaegiswil, Switzerland). The microfluidic impedance flow cytometer is a refined device based on the technology of Gawad et al. (36,39), Cheung et al. (18), and Schade-Kampmann et al. (51). Function generators and radio-frequency lock-in amplifiers have been replaced by a custom-tailored high-performance signal processing board for modulation and demodulation of the measurement signal using FPGA (Field Programmable Gate Array) technology and DAC (Digital-to-Analog Conversion) as well as ADC (Analog-to-Digital Conversion) converters. All electronic and fluidic components have been incorporated in a prototype device with easy chip exchange and automated sample loading and system cleaning procedures. The heart of the cytometer is a microfluidic chip supplied with two pairs of parallel facing microelectrodes that allow for differential measurements. The standard microfluidic chip's channel diameter is 20 μm, where a single cell suspension of 1–10 million cells/ml liquid flows through at a velocity of 6–24 cm/s during measurements. Simultaneous application of up to four different frequencies to the electrodes and recording of amplitude and phase permit multiparametric measurements of single cells with the IFC prototype, similar to fluorescence flow cytometry analyses. The built-in signal processing board sends demodulated measurement data through an USB connection to a PC running Matlab (Mathworks, Natick, MA) based control and analysis software. The obtained data are converted into the standard FCS3.0-format and can thus be analyzed with commercially available flow cytometry software.

Directly measurable parameters include impedance amplitude (R) and angle (or phase, P). Hoffman et al. defined opacity as the ratio of the impedance magnitude at a high fre-

Table 2. Recent progress in microfluidic impedance-based flow cytometry

PARTICLES ANALYZED	TECHNOLOGY	RESULTS	DEMONSTRATED DETECTION RATE	REFS.
Phytoplankton	Co-planar electrodes in glass and PDMS microchannel	327 kHz and 6 MHz discrimination between three kinds of fluorescent algae	–	(69)
Microspheres	Low reflectance RF reflectometry; parallel facing electrodes in glass and PDMS microchannel	Discrimination of beads based on size	5,000/s	(65)
Microspheres; pollen	Multi-channel Coulter counter with common sample reservoir	Four parallel microchannels: gives counting efficiency improved 300% over single-channel Coulter counter	–	(67,68)
Microspheres; yeast cells	Adjustable aperture and focusing through low-conductivity sheath flows; co-planar microelectrodes in PDMS microchannels	20 μm Microspheres and 5 μm yeast cells analyzed using the same chip design	1,000/s	(64)
Microspheres; yeast cells; CHO cells	Co-planar electrodes; microwave frequency measurements (1.5–2 GHz)	Size discrimination of particles	400–600 μm/s (beads)	(66)
Microspheres; erythrocytes; leukocytes	Polyelectrolyte salt-bridge electrodes	Velocity-independent signal amplitude even at the speed of 100 mm/s	1,000/s	(72)
Erythrocytes	Parallel facing electrodes; maximum length sequence technique for broadband impedance spectroscopy	Proof of concept for broadband measurement	–	(79)
Erythrocytes; modified erythrocytes	Parallel facing electrodes in glass and polyimide microchannel	Multifrequency measurements to distinguish modified erythrocytes	1,000/min	(18)
Babesia bovis infected erythrocytes	Co-planar electrodes in SU-8 and PDMS microchannel	Discrimination from non-infected cells at 8.7 MHz; parasitized cells have higher membrane permeability	–	(71)
Saponin-treated erythrocytes; white blood cell differential count	Parallel facing electrodes in glass and polyimide microchannel	Neutrophil-monocyte-lymphocyte discrimination at 573 kHz and 1.7 MHz	~100/s	(52)
Erythroleukemia cells	Protein-functionalized pore	Duration of the current pulse indicates cell transit time and specificity of protein–protein interactions in the pore	~100/min	(122)
Adipocyte and monocyte differentiation	Parallel facing electrodes in glass and polyimide microchannel	Opacity difference between fibroblasts and differentiated adipocytes at 8 and 14 MHz and between monocytes and differentiated dendritic cells at 14 MHz	200–1,000/min	(51)
Jurkat cell apoptosis	Parallel facing electrodes in glass and polyimide microchannel	Cycloheximide-induced apoptosis of Jurkat cells at 12 MHz	200–1,000/min	(51)
Yeast growth curve	Parallel facing electrodes in glass and polyimide microchannel	Yeast growth at 8 MHz	200–1,000/min	(51)

Table 2. Recent progress in microfluidic impedance-based flow cytometry (Continued)

PARTICLES ANALYZED	TECHNOLOGY	RESULTS	DEMONSTRATED DETECTION RATE	REFS.
CD4 T-Lymphocytes	Parallel facing electrodes in glass and polyimide microchannel	Beads coated with CD4 antibody used to label the $CD4^+$ T-cells, opacity measured (10 MHz and 503 kHz)	~100/s	(110)
Macrophage differentiation	Parallel facing electrodes in glass and benzocyclobutene microchannel	Macrophage differentiation (8 MHz)	2,000–20,000/min	This publication, Figure 3
MCF-7 cell death	Parallel facing electrodes in glass and benzocyclobutene microchannel	Cell viability (2 MHz)	2,000–20,000/min	This publication, Figure 4; (111)
Schwann cells RN22 membrane potential; intracellular free calcium	Parallel facing electrodes in glass and benzocyclobutene microchannel	Membrane potential (4 MHz); Intracellular free calcium (6 MHz)	2,000–20,000/min	This publication, Figures 5 and 6; (111)
Blood cell discrimination	Parallel facing electrodes in glass and benzocyclobutene microchannel	Erythrocyte and leukocyte discrimination (6 MHz)	2,000–20,000/min	This publication, Figure 7
Bacteria and yeast viability	Parallel facing electrodes in glass and benzocyclobutene microchannel	*Bacillus* and *Saccharomyces* strains (viability discrimination at 10 MHz)	2,000–20,000/min	This publication, Figure 8

quency to a low frequency ($|Z_{high}|/|Z_{low}|$) (45). It is a measure of the difference in particle resistivity at high and low frequency. Opacity can be used to normalize the data for both cell size and cell position between the measurement electrodes in the microfluidic channel (39). Relative opacity (RO) was defined by Hoffman et al. (45) as the ratio of the cell opacity to polymer microsphere opacity. In this article, the term RO is defined as the ratio of the impedance magnitude at a high frequency to a low frequency. Relative phase (PO) is defined as the difference of phase at a high frequency to a low frequency. In the examples presented below low frequency reference values for RO and PO were those measured at 0.5 MHz.

All further technical and experimental details are specified in the figure captions.

Cell Lines

Cell differentiation. Changes of the membrane capacitance or cytoplasmic conductivity are often closely related to cell differentiation processes. In some cases, no fluorescent dyes or other biomarkers are available for visualization. Moreover, staining or preparation in general might alter cell behavior or influence differentiation. This can be avoided or at least reduced by label-free techniques. Impedimetric discrimination of 3T3-fibroblasts and differentiated adipocytes, as well as discrimination of blood monocytes and differentiated dendritic cells, have already been shown by Schade-Kampmann et al. (51). Figure 3 presents data illustrating the discrimination of HL-60 myoblasts differentiating to macrophages recorded at 8 MHz, and demonstrates that impedance microflow cytometry can provide a valuable alternative to study such processes.

Multiparametric impedance analysis of eukaryotic cell viability and physiology. The possibility to measure each individual cell at different discrete frequencies enables multiparametric analysis. The multidimensional data for each individual cell can potentially be used to distinguish simultaneously between different cell physiological states. In this label-free technique, cells within the same sample can be indentified for cell death and changes of membrane potential or intracellular free Ca^{2+} $[Ca^{2+}]_i$ (111).

Multiparametric flow cytometric impedance analysis of cell death. Cell culture quality control is a procedure conducted in the daily routine of cell culture maintenance. A label-free approach to validate cell death is ideal for checking cellular conditions in a running cell culture. Such tests could be implemented into the sterile conditions of bioreactors for continuous monitoring. This is of special importance particularly for on-line process control in the biotechnology industry. The tested cells could be redirected and further cultured without major disruption. A possible application for this might be routine viability tests in yeast fermentations in breweries (see section "Micro-organisms").

Cell death analysis on MCF-7 breast cancer cells has also been performed. Cells were analyzed before and after treatment with ethanol (EtOH) (70%, 2 min) to induce cell death. Cell

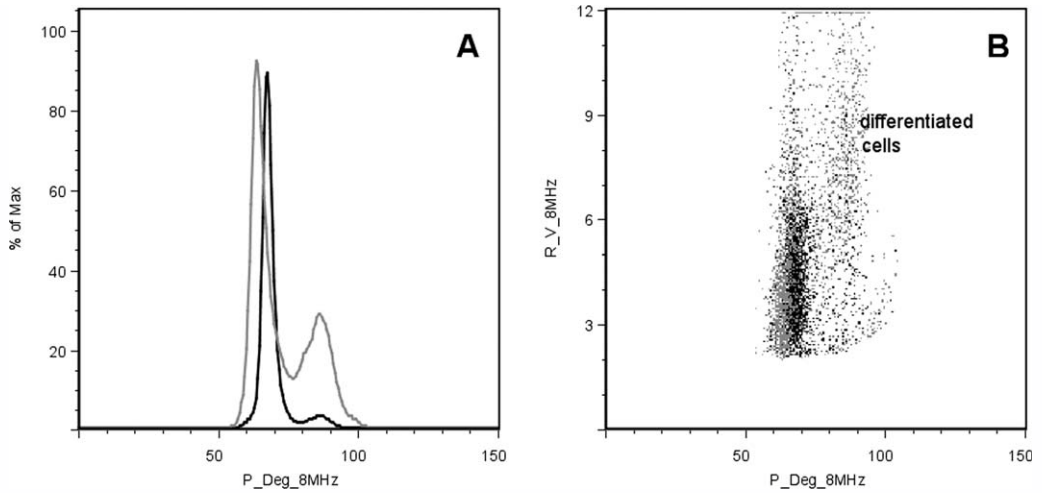

Figure 3. Differentiation of HL-60 myoblast cells to macrophages. Display of IFC data at 8 MHz for HL-60 cell differentiation induced by TPA (12-O-tetradecanoylphorbol-13-acetate). Normal HL-60 cells and partially differentiated cells are measured sequentially and datasets are superimposed (black: untreated cells, gray: partially differentiated cells). **A**: Histogram of total cell count versus phase angle (*P*). **B**: Corresponding dot plot of impedance amplitude (*R*) and phase (*P*) showing the phase shift of differentiated cells (gray dots). HL-60 cells (ATCC CCL-240) were incubated for 48 h at 37°C, 5% CO_2 in RPMI medium supplemented with 10% fetal calf serum (both AMIMED, Bioconcept, Allschwil, Switzerland) with 16 nM TPA (Sigma, Buchs, Switzerland) (138). Adherent cell fraction (about 70%) was removed by scraping and cells were measured in PBS (AMIMED) at two simultaneous frequencies (0.5 and 8 MHz). Data were analyzed by FlowJo 7.5.5 (Tree Star, Ashland, OR). [Reprinted from poster P-1-133 at DGFZ meeting 2008 in Bremen (www.dgfz.org)].

death was verified in an aliquot of the samples using flow cytometry and propidium iodide (PI) staining. At this time point, most of the cells had died and were thus PI positive. In Figure 4, dead cells were mixed with viable cells in a 1:1 ratio and analyzed by impedance flow cytometry (IFC) at multiple frequencies ranging from 0.5 MHz to 15 MHz. The example demonstrates that using microfluidic IFC, dead cells (bold lines) can be clearly distinguished from viable cells (gray lines) at different frequencies. At each frequency, two primary parameters were measured (P = angle, R = amplitude). The two bottom rows (PO = relative angle, RO = opacity) are derived parameters and were obtained by subtraction or division of P or R values, respectively, measured at a given frequency by the values obtained at 0.5 MHz. This data shows that dead cells can easily be distinguished by the parameter P and PO at various frequencies and that cell death estimation by IFC (determined by phase shift at 6 MHz) correlates with data from FCM (Fig. 4B).

Discrimination of cell death and changes in cell physiology. Figure 4A also illustrates the high level of multiplexicity one can obtain when analyzing the impedance at multiple frequencies. Here, 14 directly measured and 12 derived values were obtained per individual cell. This highly multiplexed approach indicates that multifrequency IFC has the potential for cytomic analysis of cell populations (112,113). This implies that different changes in cell physiology are reflected by different changes in the impedance spectrum.

To illustrate that multifrequency IFC can be used to distinguish various cell physiological states, cells were treated either with EtOH to induce cell death, with the potassium ionophore Valinomycin to depolarize the trans-membrane potential, or with the Br,Ca-Ionophore A23187 to increase $[Ca^{2+}]_i$. Changes in the membrane potential or $[Ca^{2+}]_i$ were verified by FCM after staining with DiBaC4 (3) or Fluo3, respectively.

As illustrated in Figure 5A, cell death, membrane potential, and $[Ca^{2+}]_i$ changes are reflected by changes of PO at different frequencies. These data can be dealt with as with regular FCM data using similar algorithms for standardization and calibration (114). Resolution parameter (Fig. 5B) or peak ratio (Fig. 5C) can be calculated and displayed to scrutinize for the best discriminatory parameters. These graphics illustrate that cell death leads to changes at different frequencies enabling their differentiation from changes induced by Valinomycin or A23187. The distinction between Valinomycin and A23187 induced responses, however, is not immediately striking. But, when combining different parameters in scattergrams (Fig. 6) it becomes clear that combinations may help to differentiate even between these responses.

It is feasible in future to use the wealth of the obtained 26-dimensional field of data to clearly separate specific responses from one another. As proposed for Cytomics in flow cytometry, one can select those parameters that can discriminate between various cell states by >95% after exhaustive hypothesis free mathematical data-mining using the wide range of measured parameters (115). Typical multivariate mathematical tools for parameter selection and reduction include discriminant analysis, principal component analysis, Classif1, neuronal networks, and others (112,115–117). This should yield optimal combinations of measured and calculated data for accurate cell characterization.

Red Blood Cells and Leukocytes

Red blood cells. Previous work has shown that modified cells can be discriminated from native cells based on changes in

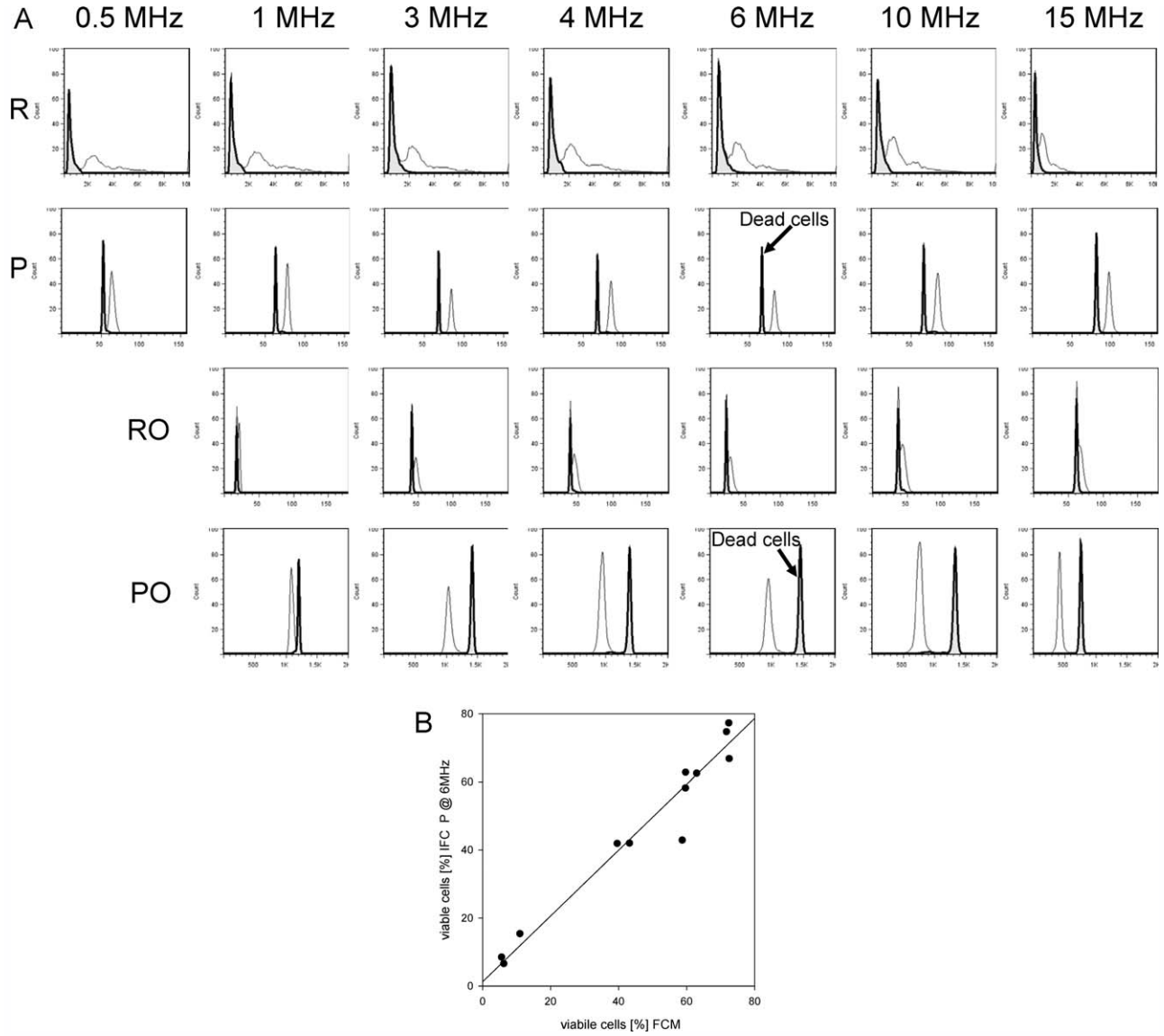

Figure 4. Analysis of cell death by multifrequency microfluidic impedance flow cytometry. **A**: Overall data display for frequencies and parameters collected by IFC at different frequencies for MCF-7 cell death induced by EtOH (70% for 2 min). Data obtained for dead cells are indicated by **bold** lines. *R* = amplitude, *P* = angle, PO = relative angle (relative angle = $\text{angle}_{\text{high frequency}} - \text{angle}_{0.5\ \text{MHz}}$), RO = opacity (opacity = $\text{amplitude}_{\text{high frequency}}/\text{amplitude}_{0.5\ \text{MHz}}$). For details, see text (section ''Multiparametric Impedance Analysis of Eukaryotic Cell Viability and Physiology). (Figure modified and reproduced from Ref. 111 with permission from the publisher). MCF-7 cells (human breast carcinoma) (ATCC HTB-22) were cultured in DMEM medium supplemented with 10% fetal calf serum (both Sigma, St. Louis, MO) at 37°C, 5% CO_2. After 10 min of treatment with EtOH (Carl Roth GmbH, Karlsruhe, Germany) (70%) almost all cells were killed (proven by FCM measurement) by propidium iodide (PI, 0.5 μg/ml; Sigma). Then, the killed cells were mixed with untreated cells at 1:1 ratio. Cells were resuspended in Ficoll (Sigma)/PBS solution (density: 1.05 g/ml, conductivity: 16.5 mS, pH 7.3) to avoid sedimentation. Frequencies analyzed are indicated in Fig. 4A top row (two sets of four frequencies were measured subsequently. Set 1 = 0.5, 1, 4, and 10 MHz; Set 2 = 0.5, 3, 6, and 15 MHz). **B**: Comparison of the percentages of dead cells obtained by FCM and IFC. Dead cells were determined through IFC by *P* value at 6 MHz (arrow in A). Cell death was measured by PI staining using FCM. The line shows the linear regression for 12 independent experiments using different viable:dead cell ratios ($P < 0.05$, $R = 0.994$).

membrane conductance or morphology. Leif et al. showed that opacity could be related to erythrocyte age, since opacity increased with increasing cell buoyant density, and buoyant density is directly related to the age of the cell (118). Cheung et al. (119) used a microfluidic impedance cytometry setup to show differentiation between a mixture of particles with submicron size resolution, and discrimination of erythrocytes with different levels of membrane and cytoplasm modification (18). Electrorotation and dielectrophoretic crossover studies (120) have shown that malarial parasite (*Plasmodium falciparum*) infected erythrocytes have a greatly increased membrane conductance in comparison to normal erythrocytes, which is a parameter which could be used for sorting of these cells. Küttel et al. (71) used a flow-through impedance-based microfluidic cytometer to detect

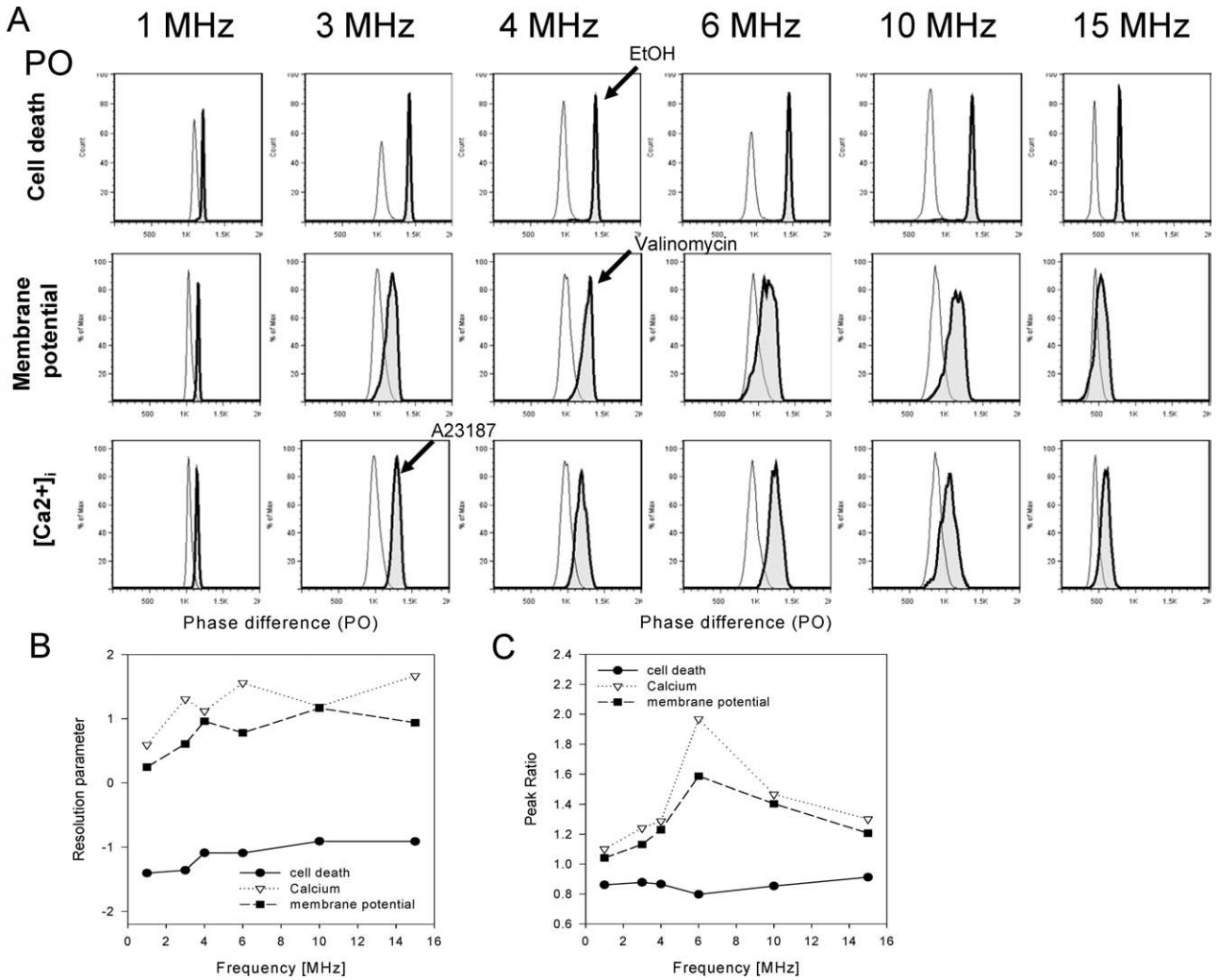

Figure 5. Discrimination of cell death, membrane potential change, and $[Ca^{2+}]_i$ changes by multifrequency IFC using phase difference (PO). **A**: Display of PO for the whole range of frequencies for three different cellular effects: cell death induced by EtOH (70% for 2 min); membrane depolarization induced by valinomycin (1 μM for 15 min); $[Ca^{2+}]_i$ changes induced by A23187 (1 μM for 15 min). Arrows and **bold** lines indicate affected cells. Thin lines indicate untreated cells. First row: cell death, data from Figure 4A. Middle and bottom row: RN22 cells were grown in DMEM medium (Sigma) supplemented with 10% horse serum (Sigma) and 5% fetal calf serum (Sigma). They were either left untreated or stimulated for 30 min with 1 μM Valinomycin (Merck, Darmstadt, Germany) to induce depolarization or with 1 μM A23187 (Merck) to induce increase in $[Ca^{2+}]_i$. Subsequently, cells were suspended in Ficoll (Sigma)/PBS solution (density: 1.05 g/ml, conductivity: 16.5 mS, pH: 7.3) for IFC measurement. As reference, cells were stained with $DiBAC_4$ or Fluo-3 for estimation of membrane potential or calcium concentration change by FCM, respectively. Instrument settings as in Figure 4A (Figure modified and reproduced from Ref. 111 with permission from the publisher). **B**: Resolution parameter ($Mean^+ - Mean^-/StandDev^+ + StandDev^-$) for PO derived for all cellular responses studied displayed versus the measured frequencies (114). **C**: Peak ratio ($Mean^+/Mean^-$) for PO parameter was calculated for each of the cellular responses studied versus the measured frequencies (114).

Babesia bovis infected RBCs. These parasitized cells also have a higher membrane permeability, and this property was used to enrich the fraction of infected cells through on-chip dielectric sorting (121).

In contrast to typical cytometry systems in which the cells should have no interactions with the walls of the pore, Carbonaro et al. (122) have used a functionalized pore to identify cells based on the interactions of their cell surface markers with the proteins on the pore surface. The pore diameter was comparable to the diameter of the erythroleukemia cells measured. The magnitude of the current pulse as the cell passes through the pore reflects the size of the cell, while the duration of the current pulse indicates cell transit time, which gives information on whether the cell-pore interactions involved specific protein–protein interactions. This label-free method to screen small numbers of cells could also be used to give quantitative information about the density of a specific cell surface receptor.

Leukocytes. Changes in specific cell membrane capacitance have been shown to correlate with the onset of induced apoptosis (123). Electrorotation and dielectrophoretic methods

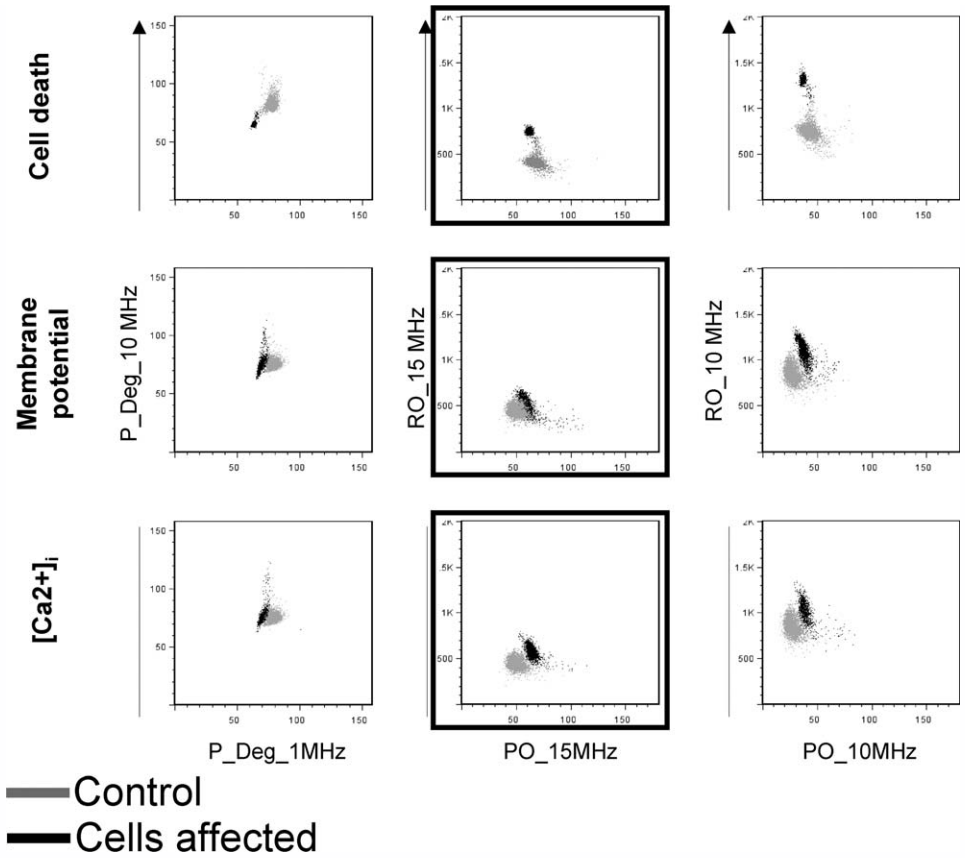

Figure 6. Multiparametric display improves distinction of cell death from membrane potential and $[Ca^{2+}]_i$ changes. Dot plots show resolution of control (gray) and stimulated cells (black) for selected parameters and frequency combinations. By means of different parameter sets, it is possible to distinguish between different cellular effects. Thus, suitable parameter and frequency patterns may be defined to determine cell-specific response. Here, three different parameters are displayed for three different cell responses. Parameter combinations that may enable distinction between cell death, change in membrane potential, and change in $[Ca^{2+}]_i$ are highlighted (Reproduced from Ref 111 with permission).

have also shown that human leukocyte subpopulations could be separated based on measurements of specific membrane capacitance values, since these values correlate with the surface morphologies of the different cell types (124). Microvilli, folds, ruffles, and other membrane features increase the total area of the plasma membrane capacitance C_{total}, where $C_{total} = \varepsilon_{mem}A/d$, ε_{mem} is the average dielectric permittivity of the membrane, A is the membrane area, and d is the membrane thickness. Complex surface morphology consequently increases the cell membrane capacitance per unit area, C_{mem}, where $C_{mem} = C_{total}/(\pi D^2)$ and D is the average cell diameter (125,126). Leukocyte subpopulations have been discriminated using electrorotation data, which correlated with the different surface morphologies of lymphocytes, monocytes, and granulocytes (124). Granulocytes and monocytes exhibit more ruffles on their surface than lymphocytes, whereas B-lymphocytes exhibit more microvilli. In addition to the effect of area, specific membrane capacitance is also a function of the membrane thickness and composition. These differences were shown to be separable factors for different leukocyte cell types. Using dielectrophoretic crossover frequency measurements, Vykoukal et al. (127) have characterized the six major WBC subpopulations (T-lymphocytes, B-lymphocytes, monocytes, neutrophils, eosinophils, and basophils). They demonstrated that the polymorphonuclear granulocytes had dielectric properties that are distinct from mononuclear lymphocytes and monocytes. A scattergram of leukocyte subpopulations in which C_{mem} is plotted versus cell radius shows that all six cell types should be separable based on dielectric properties. In a microfluidic impedance-based detection system, Holmes et al. (52) demonstrated a WBC differential count, identifying neutrophils, monocytes, and lymphocytes. Upon exposing whole blood to a solution of saponin in formic acid for 6 s, erythrocytes were lysed into fragments which did not interfere with the impedance measurement of the leukocytes. The brief saponin treatment improved the separability of these cell types by increasing the membrane capacitance of monocytes, as correlated with electrorotation analysis.

Multifrequency analysis can be used for a blood differential cell count using only pretreatment to lyse RBCs. Figure 7 shows the discrimination of WBC subpopulations using a measurement at 6 MHz.

Micro-organisms

A sweep through discrete frequencies could be used to characterize the dielectric properties of a cell population. Si-

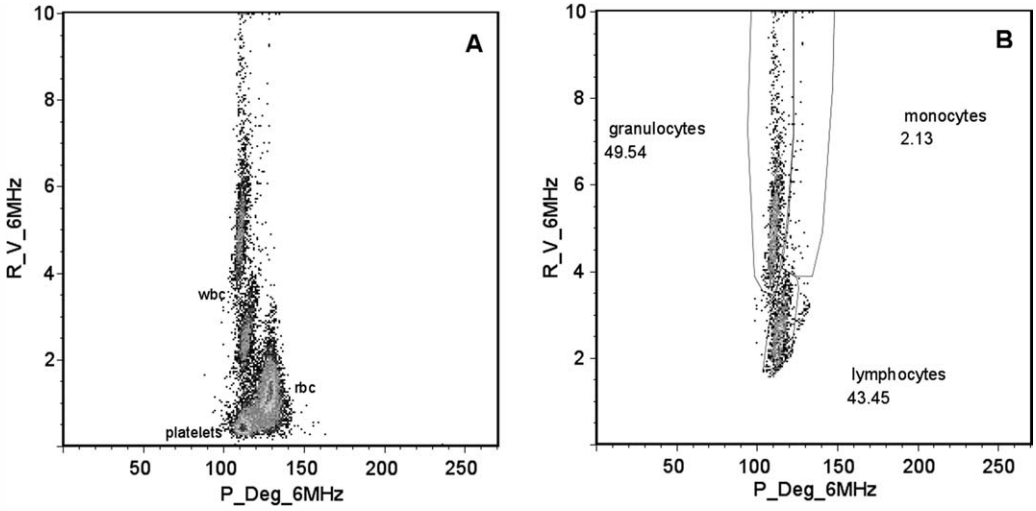

Figure 7. Blood differential cell count. IFC measurement of partially lysed and centrifuged whole blood at 6 MHz. **A**: In the *P* and *R* dot plot, residual platelets, residual RBCs, and WBCs are seen as distinct subpopulations. **B**: Shows the same plot with RBC's and platelets gated out and the fractions of the WBC subpopulations determined. Gates for WBC populations were applied according to MACS® labeled and sorted control populations (data not shown). Whole blood was collected by venipuncture from healthy adult volunteer donors into sterile tubes containing EDTA. Whole blood was diluted in 150 mM NH_4Cl-buffer (Miltenyi Biotec, Bergisch Gladbach, Germany), which leads to a partial lysis of RBCs and sample was subsequently centrifuged and diluted in PBS for measurement at two simultaneous frequencies (0.5 and 6 MHz). [reprinted from poster P-1-133 at DGFZ meeting 2008 in Bremen (www.dgfz.org)].

multaneous measurement at several discrete frequencies or a broadband measurement can be used to interrogate the dielectric properties of single cells. Systems with these capabilities are suitable for general laboratory analysis. Alternatively, simple, dedicated systems could be developed for specific applications.

For the solution conductivity and frequency range commonly used (>100 kHz), the electrode's double layer capacitance and electrode polarization still permit impedance measurements for the cell size and β-relaxation of the bacteria and yeasts. Until recently, impedance-based analysis systems provided only total cell counts, density, and size information, but failed in characterizing these kinds of cells any further. Preliminary results obtained with a prototype, derived from an optimized device described by Schade-Kampmann et al. (51), indicate its suitability for viability studies, in which the cells generally need to be labeled. Figure 8, for example, shows viability analyses in which heat-inactivated and viable cells of *Bacillus* and *Saccharomyces* strains were discriminated at 10 MHz. These findings emphasize the potential of a simple instrument for micro-organism viability studies using high frequency

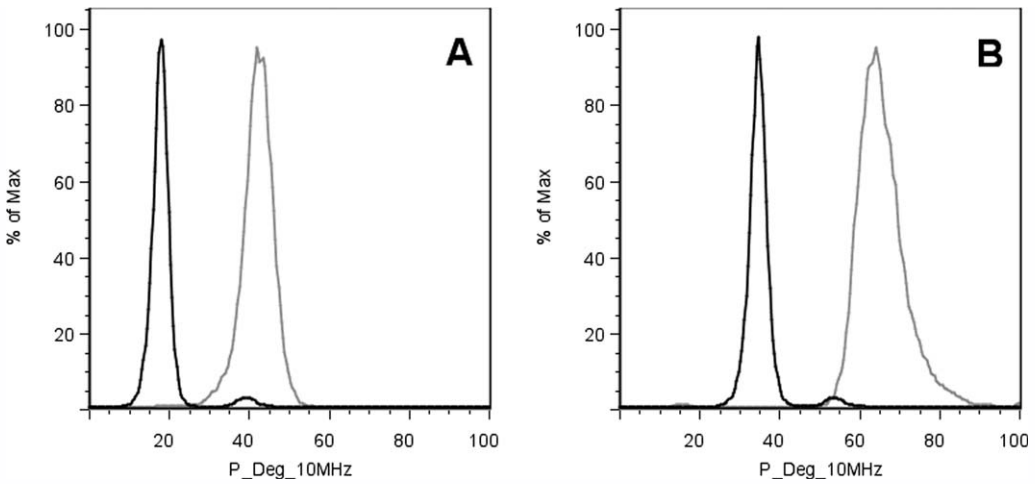

Figure 8. Cell viability determination. Impedance phase (*P*) measurement overlays of viable (gray) and heat-inactivated (black) *Saccharomyces cerevisiae* (**A**) and *Bacillus megaterium* cells (**B**) are shown in histograms at 10 MHz. Viable and dead yeast and bacterial cells can be clearly distinguished by an impedance phase shift. *Saccharomyces cerevisiae* ATCC 9080 were cultured in YPD and *Bacillus megaterium* in LB medium (both from Sigma), both overnight at 30°C and 250 rpm. Cells were heat-inactivated at 70°C for 10 min in a water bath, checked by Methylene blue staining (Sigma, Buchs, Switzerland), and diluted in 0.5× PBS for measurement at two simultaneous frequencies (0.5 and 10 MHz). [Reprinted from poster P-1-133 at DGFZ meeting 2008 in Bremen (www.dgfz.org)].

Table 3. Recent progress in microfluidic sorting

PARTICLES ANALYZED	SORTING METHOD	DEMONSTRATED SORTING RATE OR MEAN FLOW RATE/SPEED	REFS.
–	On-chip PDMS valves	Response time: ~5 ms	(128)
Microspheres	DEP gates to divert and concentrate particles	52 nl/min	(129)
Microspheres	DEP switches	300/s	(130)
Microspheres; bacteria	Laser-activated thermoreversible polymer	0.3/s	(132,133)
Microspheres; *E. coli*	Piezoelectric actuator in PDMS channel on glass substrate	Response time: 0.1–1 ms Sorting: 330/s, up to 1,000/s	(135)
Microspheres; E-GFP expressing β-cells	Piezoelectric transducer—acoustic radiation force acts on the interface between two fluids of different density	Switch time: 0.36 s Sorting: 3/s	(136)
Droplet-encapsulated cells	DEP, fluorescence-activated droplet sorter	2,000/s	(131)
H2B-GFP expressing HeLa cells	Optical force switching	Response time: 2–4 ms Sorting: 1,000–280,000/h	(134)

characterization and thus provide a sound base for a future commercialization of this technology.

Future Challenges

High-speed continuous sorting remains a challenge for microfluidic flow cytometry. Sorting can be actuated through electrokinetic, magnetic, optical, or hydrodynamic forces. Electro-osmotic flows can switch the flow between collection and waste outlets by applying DC electric fields. However, the throughput can be relatively low at the cost of high power consumption (128). DEP gates have been used to divert and concentrate particles at flow rates ~52 nl/min and high concentration factor (129), and DEP switches have been used to sort particles at a rate of 300/s (130). DEP has also been used to sort droplet-encapsulated cells in a microfluidic fluorescence-activated sorter (131) at a rate of 2,000/s. A laser-activated thermoreversible polymer was used for flow switching to sort bacteria from microspheres (132), although the throughput achieved was on the order of 0.3 cells/s (133). Optical forces have also been used to control cell routing on microfluidic chips, with response times on the order of 2–4 ms (134). Flow switching can also be accomplished through on-chip PDMS valves, but the response time, on the order of 5 ms, will be limited by the mechanical compliance of the valve (128).

Chen et al. (135) have developed a piezoelectric actuator which is embedded into the microchannel to deflect single cells. The piezoelectric actuator has a response time on the order of 0.1–1 ms. The deflection can be tuned by controlling the magnitude and waveform of the input voltage, and sorting of more than 1,000 particles/s can be achieved. Johansson et al. (136) have also sorted cells using an piezoelectric transducer on the microfluidic channel bottom. In this case, the acoustic radiation force acts on the interface between two fluids of different density, so that large particle displacements, up to 100 μm for a 3 MHz system can be achieved, although the switch time of 0.36 s corresponds to a sorting speed of 3 particles/s. In any case, it is of course conceivable to combine the described impedance analysis functionality, which can already achieve considerable event rates, with the sorting capability of conventional FACS devices and thus offer powerful solutions for applications demanding a label-free approach.

A summary of recent progress in microfluidic particle sorting is presented in Table 3.

Other challenges may include on-chip sample preparation, so that unprocessed whole blood or other samples may be directly placed into the flow cytometer. Such labs-on-a-chip would be very attractive for point of care diagnostics (e.g., $CD4^+$ cell counting) or rapid screening tests in different applications. Depending on the sample and cells of interest, hydrodynamic filtration may be used for size separation or on-chip preconcentration (84,106). Integration of on-chip cell washing, incubation with stains/reagents for multiparametric analysis, or similar steps would be straightforward (137). Further optimization of fluidic interconnect to minimize dead volumes will also improve the usability of such systems for analysis of small samples.

Conclusions

Microfabrication technologies for microfluidic systems have greatly matured over the past decade, with chips fabricated in glass, photosensitive polymers (polyimide, SU-8), elastomers (PDMS soft lithography), and hot-embossed polymers. Recent work has thus focused on incorporating new understanding of microscale flow phenomena to improve sample focusing within the cytometer and, thus, improve sensitivity. Although many standard flow-based assays have been

developed using microfluidic technology, the miniaturized flow cytometers have not yet integrated the multiparameter analyses (multiple fluorescence colors as well as morphological features) afforded by conventional flow cytometers. Future integration of impedance measurements with optical or other analysis modalities could bring added functionality to laboratory systems. Instead of targeting the high throughput (up to 10,000 cells/s) of conventional systems, microfluidic systems can bring improved sensitivity for detecting and analyzing rare cells within small samples using a label-free method, bringing added convenience. The fact that the analysis does not require prior cell labeling significantly shortens and simplifies sample preparation. Another advantage of this system is that a single instrumentation platform can readily accommodate many different chips, the design of which can be easily adapted for different applications. The diameter of the microfluidic channels could be optimized to the size of the analyzed cells (micro-organisms, mammalian cells, or other particles) for maximum sensitivity.

Label-free, impedance-based microfluidic systems have already been used to analyze viability of yeast and bacteria; to discriminate between WBCs in a differential count; to detect parasite-infected RBCs. Recent work in a microfluidic flow-through system has shown that discrete frequencies can be used to analyze the differentiation of adipocytes and monocytes, demonstrating the potential of the impedance-based technology. Multifrequency analysis, in addition to distinguishing cell types, could also be used to examine on-target and off-target effects during drug screening on a mixed cell population. Characterization and enrichment of stem cells for therapeutic use would benefit from label-free techniques and could be a future application among others. Dedicated, simple systems for specific applications are expected to reach the market within the next 5 years.

Acknowledgments

The authors thank Florian David at TU Braunschweig for providing them the *Bacillus megaterium* strain and Adrian Ziswiler at Leister Process Technologies for technical support with the impedance cytometer prototype. The authors MDB, GSK, and MH are employees of the company Leister Process Technologies, Axetris Division, which supplied the impedance cytometer prototype for the analyses performed at TRM and the Cardiac Center at the University of Leipzig.

Literature Cited

1. Sims CE, Allbritton NL. Analysis of single mammalian cells on-chip. Lab Chip 2007;7:423–440.
2. Bold A, Wurth R, Keller T, Trahorsch U, Voigt P, Schubert S, Sack U. Low-cost enumeration of $CD4^+$ T cells using a density-based negative selection method (RosetteSep) for the monitoring of HIV-infected individuals in non-OECD countries. Cytometry Part A 2008;71A:28–35.
3. Cheng X, Gupta A, Chen C, Tompkins RG, Rodriguez W, Toner M. Enhancing the performance of a point-of-care $CD4^+$ T-cell counting microchip through monocyte depletion for HIV/AIDS diagnostics. Lab Chip 2009;9:1357–1364.
4. Cheng X, Irimia DM, Dixon M, Ziperstein JC, Demirci U, Zamir L, Tompkins RG, Toner M, Rodriguez WR. A microchip approach for practical label-free $CD4^+$ T-cell counting of HIV-infected subjects in resource-poor settings. J Acquir Immune Def Synd 2007;45:257–261.
5. Greve B, Weidner J, Cassens U, Odaibo G, Olaleye D, Sibrowski W, Reichelt D, Nasdala I. A new affordable flow cytometry based method to measure HIV-1 viral load. Cytometry Part A 2009;75A:199–206.
6. Moon S, Keles HO, Ozcan A, Khademhosseini A, Hæggstrom E, Kuritzkes D, Demirci U. Integrating microfluidics and lensless imaging for point-of-care testing. Biosens Bioelectron 2009;24:3208–3214.
7. Lizard G. Diagnosing HIV infection using flow cytometry: From antigenic analyses to a specifically dedicated bead-based assay to measure viral load. Cytometry Part A 2009;75A:172–174.
8. Barnett D, Walker B, Landay A, Denny T. CD4 immunophenotyping in HIV infection. Nat Rev Microbiol 2008;6 (11 Suppl):S7–S15.
9. Zhang H, Chon CH, Pan X, Li D. Methods for counting particles in microfluidic applications. Microfluid Nanofluid 2009;7:739–749.
10. Ymeti A, Li X, Lunter B, Breukers C, Tibbe A, Terstappen L, Greve J, Ymeti A, Li X, Lunter B, Breukers C, Tibbe AG, Terstappen LW, Greve J. A single platform image cytometer for resource-poor settings to monitor disease progression in HIV infection. Cytometry Part A 2007;71A:132–142.
11. Shapiro H, Perlmutter N. Personal cytometers: Slow flow or no flow? Cytometry Part A 2006;69A:620–630.
12. Mandy F, Janossy G, Bergeron M, Pilon R. Affordable CD4 T-cell enumeration for resource-limited regions: A status report for 2008. Cytometry B Clin Cytom 2008;74B (Suppl 1):S27–S39.
13. Chung TD, Kim HC. Recent advances in miniaturized microfluidic flow cytometry for clinical use. Electrophoresis 2007;28:4511–4520.
14. Shapiro H, Mandy F. Cytometry in malaria: Moving beyond Giemsa. Cytometry Part A 2007;71A:643–645.
15. Hong J, Edel JB, deMello AJ. Micro- and nanofluidic systems for high-throughput biological screening. Drug Discov Today 2009;14:134–146.
16. Lima R, Wada S, Tsubota K, Yamaguchi T. Confocal micro-PIV measurements of three-dimensional profiles of cell suspension flow in a square microchannel. Meas Sci Technol 2006;17:797–808.
17. Krutzik PO, Crane JM, Clutter MR, Nolan GP. High-content single-cell drug screening with phosphospecific flow cytometry. Nat Chem Biol 2008;4:132–142.
18. Cheung K, Gawad S, Renaud P. Impedance spectroscopy flow cytometry: On-chip label-free cell differentiation. Cytometry Part A 2005;65A:124–132.
19. Galanzha E, Shashkov E, Tuchin V, Zharov V. In vivo multispectral, multiparameter, photoacoustic lymph flow cytometry with natural cell focusing, label-free detection and multicolor nanoparticle probes. Cytometry Part A 2008;73A:884–894.
20. Lee E, Kidder LH, Kalasinsky VF, Schoppelrei JW, Lewis EN. Forensic visualization of foreign matter in human tissue by near-infrared spectral imaging: Methodology and data mining strategies. Cytometry Part A 2006;69A:888–896.
21. Rappaz B, Barbul A, Emery Y, Korenstein R, Depeursinge C, Magistretti P, Marquet P. Comparative study of human erythrocytes by digital holographic microscopy, confocal microscopy, and impedance volume analyzer. Cytometry Part A 2008;73A:895–903.
22. Steiner G, Küchler S, Hermann A, Koch E, Salzer R, Schackert G, Kirsch M. Rapid and label-free classification of human glioma cells by infrared spectroscopic imaging. Cytometry Part A 2008;73A:1158–1164.
23. Watson DA, Brown LO, Gaskill DF, Naivar M, Graves SW, Doorn SK, Nolan JP. A flow cytometer for the measurement of Raman spectra. Cytometry Part A 2008;73A:119–128.
24. Chung A, Karlan S, Lindsley E, Wachsmann-Hogiu S, Farkas DL. In vivo cytometry: A spectrum of possibilities. Cytometry Part A 2006;69A:142–146.
25. Fu AY, Spence C, Scherer A, Arnold FH, Quake SR. A microfabricated fluorescence-activated cell sorter. Nat Biotech 1999;17:1109–1111.
26. Wolff A, Perch-Nielsen IR, Larsen UD, Friis P, Goranovic G, Poulsen CR, Kutter JP, Telleman P. Integrating advanced functionality in a microfabricated high-throughput fluorescent-activated cell sorter. Lab Chip 2003;3:22–27.
27. Kostner S, Vellekoop MJ. Cell analysis in a microfluidic cytometer applying a DVD pickup head. Sens Actuat B Chem 2008;132:512–517.
28. Spegel C, Heiskanen A, Skjolding LHD, Emnéus J. Chip based electroanalytical systems for cell analysis. Electroanalysis 2008;20:680–702.
29. Pauly H, Schwan HP. Uber die Impedanz einer Suspension von kugelformigen Teilchen mit einer Schale. Z Naturforsch 1959;14:125–131.
30. Asami K, Yonezawa T, Wakamatsu H, Koyanagi N. Dielectric spectroscopy of biological cells. Bioelectrochem Bioenergy 1996;40:141–145.
31. Cheng X, Liu Y-s, Irimia D, Demirci U, Yang L, Zamir L, Rodriguez WR, Toner M, Bashir R. Cell detection and counting through cell lysate impedance spectroscopy in microfluidic devices. Lab Chip 2007;7:746–755.
32. Bao N, Wang J, Lu C. Recent advances in electric analysis of cells in microfluidic systems. Anal Bioanal Chem 2008;391:933–942.
33. Gascoyne PRC, Vykoukal J. Particle separation by dielectrophoresis. Electrophoresis 2002;23:1973–1983.
34. Kaler KV, Jones TB. Dielectrophoretic spectra of single cells determined by feedback-controlled levitation. Biophys J 1990;57:173–182.
35. Wang XB, Vykoukal J, Becker FF, Gascoyne PRC. Dielectrophoretic separation of cancer cells from blood. IEEE T Ind Appl 1998;33:670–678.
36. Gawad S, Schild L, Renaud P. Micromachined impedance spectroscopy flow cytometer for cell analysis and particle sizing. Lab Chip 2001;1:76–82.
37. Sun T, Morgan H. Single-cell microfluidic impedance cytometry: A review. Microfluid Nanofluid 2010. Doi: 10.1007/s10404–010-0580–9.
38. Hoffman RA, Britt WB. Flow-system measurement of cell impedance properties. J Histochem Cytochem 1979;27:234–240.
39. Gawad S, Cheung KC, Seger U, Bertsch A, Renaud P. Dielectric spectroscopy in a micromachined flow cytometer: Theoretical and practical considerations. Lab Chip 2004;4:241–251.

40. Sun T, Gawad S, Green NG, Morgan H. Dielectric spectroscopy of single cells: Time domain analysis using Maxwell's mixture equation. J Phys D: Appl Phys 2007;1:1.
41. Sun T, Green NG, Morgan H. Analytical and numerical modeling methods for impedance analysis of single cells on-chip. Nano 2008;3:55–63.
42. Huh D, Gu W, Kamotani Y, Grotberg JB, Takayama S. Microfluidics for flow cytometric analysis of cells and particles. Physiol Meas 2005;26:R73–R98.
43. Whitesides G, Ostuni E, Takayama S, Jiang X, Ingber DE. Soft lithography in biology and biochemistry. Annu Rev Biomed Eng 2001;3:335–373.
44. Coulter W, Hogg W. Signal Modulated Apparatus for Generating and Detecting Resistance and Reactive Changes in a Modulated Current Passed for Particle Classification and Analysis. US Patent3,502,974. 1970.
45. Hoffman RA, Johnson TS, Britt WB. Flow cytometric electronic direct current volume and radiofrequency impedance measurements of single cells and particles. Cytometry 1981;1:377–384.
46. Leif RC, Thomas RA, Yopp TA, Watson BD, Guarino VR, Hindman DHK, Lefkove N, Vallarino LM. Development of instrumentation and fluorochromes for automated multiparameter analysis of cells. Clin Chem 1977;23:1492–1498.
47. Thomas RA, Yopp TA, Watson BD, Hindman DHK, Cameron BF, Leif SB, Leif RC, Roque L, Britt W. Combined optical and electronic analysis of cells with the AMAC transducers. J Histochem Cytochem 1977;25:827–835.
48. Leif RC, Cayer ML, Dailey W, Stribling T, Gordon K. The use of a spherical multiparameter transducer for flow cytometry. Cytometry 1995;20:185–190.
49. Li Q, Gerena L, Xie L, Zhang J, Kyle D, Milhous W. Development and validation of flow cytometric measurement for parasitemia in cultures of *P. falciparum* vitally stained with YOYO-1. Cytometry Part A 2007;71A:297–307.
50. Sandhaus LM, Osei ES, Agrawal NN, Dillman CA, Meyerson HJ. Platelet counting by the coulter LH 750. Sysmex XE 2100, and Advia 120. Am J Clin Pathol 2002;118:235–241.
51. Schade-Kampmann G, Huwiler A, Hebeisen M, Hessler T, Berardino MD. On-chip non-invasive and label-free cell discrimination by impedance spectroscopy. Cell Prolif 2008;41:830–840.
52. Holmes D, Pettigrew D, Reccius CH, Gwyer JD, Berkel Cv, Holloway J, Davies DE, Morgan H. Leukocyte analysis and differentiation using high speed microfluidic single cell impedance cytometry. Lab Chip 2009;9:2881–2889.
53. Xia M, Huang R, Witt K, Southall N, Fostel J, Cho M, Jadhav A, Smith C, Inglese J, Portier C. Compound cytotoxicity profiling using quantitative high-throughput screening. Environ Health Perspect 2008;116:284–291.
54. Ge Y, Deng T, Zheng X. Dynamic monitoring of changes in endothelial cell-substrate adhesiveness during leukocyte adhesion by microelectrical impedance assay. Acta Biochim Biophys Sin (Shanghai) 2009;41:256–262.
55. Xi B, Yu N, Wang X, Xu X, Abassi Y. The application of cell-based label-free technology in drug discovery. Biotechnol J 2008;3:484–495.
56. Linderholm P, Bertsch A, Renaud P. Resistivity probing of multilayered tissue phantoms using microelectrodes. Physiol Meas 2004;3:645–658.
57. Linderholm P, Braschler T, Vannod J, Barrandon Y, Brouard M, Renaud P. Two-dimensional impedance imaging of cell migration and epithelial stratification. Lab Chip 2006;6:1155–1162.
58. Krinke D, Jahnke H, Pänke O, Robitzki A. A microelectrode-based sensor for label-free in vitro detection of ischemic effects on cardiomyocytes. Biosens Bioelectron 2009;24:2798–2803.
59. Jahnke H, Rothermel A, Sternberger I, Mack T, Kurz R, Pänke O, Striggow F, Robitzki A. An impedimetric microelectrode-based array sensor for label-free detection of tau hyperphosphorylation in human cells. Lab Chip 2009;9:1422–1428.
60. Rothermel A, Nieber M, Müller J, Wolf P, Schmidt M, Robitzki A. Real-time measurement of PMA-induced cellular alterations by microelectrode array-based impedance spectroscopy. Biotechniques 2006;41:445–450.
61. Wolf P, Rothermel A, Beck-Sickinger A, Robitzki A. Microelectrode chip based real time monitoring of vital MCF-7 mamma carcinoma cells by impedance spectroscopy. Biosens Bioelectron 2006;24:253–259.
62. O'Connor JE, Martínez A, Castell JV, Gómez-Lechón MJ. Multiparametric characterization by flow cytometry of flow-sorted subpopulations of a human hepatoma cell line useful for drug research. Cytometry Part A 2005;63A:48–58.
63. Rodriguez-Trujillo R, Castillo-Fernandez O, Garrido M, Arundell M, Valencia A, Gomila G. High-speed particle detection in a micro-Coulter counter with two-dimensional adjustable aperture. Biosens Bioelectron 2008;24:290–296.
64. Rodriguez-Trujillo R, Mills C, Samitier J, Gomila G. Low cost micro-Coulter counter with hydrodynamic focusing. Microfluid Nanofluid 2007;3:171–176.
65. Wood DK, Requa MV, Cleland AN. Microfabricated high-throughput electronic particle detector. Rev Sci Instrum 2007;78:104301–104306.
66. Nikolic-Jaric M, Romanuik SF, Ferrier GA, Bridges GE, Butler M, Sunley K, Thomson DJ, Freeman MR. Microwave frequency sensor for detection of biological cells in microfluidic channels. Biomicrofluidics 2009;3:034103.
67. Jagtiani AV, Zhe J, Hu J, Carletta J. Detection and counting of micro-scale particles and pollen using a multiaperture Coulter counter. Meas Sci Technol 2006;17:1706.
68. Zhe J, Jagtiani A, Dutta P, Hu J, Carletta J. A micromachined high throughput Coulter counter for bioparticle detection and counting. J Micromech Microeng 2007;17:304.
69. Benazzi G, Holmes D, Sun T, Mowlem MC, Morgan H. Discrimination and analysis of phytoplankton using a microfluidic cytometer. IET Nanobiotechnol 2007;1:94–101.
70. Holmes D, She JK, Roach PL, Morgan H. Bead-based immunoassays using a microchip flow cytometer. Lab Chip 2007;7:1048–1056.
71. Küttel C, Nascimento E, Demierre N, Silva T, Braschler T, Renaud P, Oliva AG. Label-free detection of Babesia bovis infected red blood cells using impedance spectroscopy on a microfabricated flow cytometer. Acta Trop 2007;102:63–68.
72. Chun H, Chung TD, Kim HC. Cytometry and velocimetry on a microfluidic chip using polyelectrolytic salt bridges. Anal Chem 2005;77:2490–2495.
73. Kim KB, Chun H, Kim HC, Chung TD. Red blood cell quantification microfluidic chip using polyelectrolytic gel electrodes. Electrophoresis 2009;30:1464–1469.
74. Joo S, Kim KH, Kim HC, Chung TD. A portable microfluidic flow cytometer based on simultaneous detection of impedance and fluorescence. Biosens Bioelectron 2010;25:1509–1515.
75. Demierre N, Braschler T, Linderholm P, Seger U, van Lintel H, Renaud P. Characterization and optimization of liquid electrodes for lateral dielectrophoresis. Lab Chip 2007;7:355–365.
76. Morgan H, Sun T, Holmes D, Gawad S, Green NG. Single cell dielectric spectroscopy. J Phys D: Appl Phys 2007;1:61.
77. Sun T, Gawad S, Bernabini C, Green NG, Morgan H. Broadband single cell impedance spectroscopy using maximum length sequences: Theoretical analysis and practical considerations. Meas Sci Technol 2007;18:2859.
78. Sun T, Holmes D, Gawad S, Green NG, Morgan H. High speed multifrequency impedance analysis of single particles in a microfluidic cytometer using maximum length sequences. Lab Chip 2007;7:1034–1040.
79. Gawad S, Sun T, Green NG, Morgan H. Impedance spectroscopy using maximum length sequences: Application to single cell analysis. Rev Sci Instrum 2007;78:054301–054307.
80. Sun T, van Berkel C, Green N, Morgan H. Digital signal processing methods for impedance microfluidic cytometry. Microfluid Nanofluid 2009;6:179–187.
81. Foster KR, Schwan HP. Dielectric properties of tissues and biological materials: A critical review. Crit Rev Biomed Eng 1989;17:25–104.
82. Sklar LA, Carter MB, Edwards BS. Flow cytometry for drug discovery, receptor pharmacology and high-throughput screening. Curr Opin Pharmacol 2007;7:527–534.
83. Sun T, Green NG, Gawad S, Morgan H. Analytical electric field and sensitivity analysis for two microfluidic impedance cytometer designs. IET Nanobiotechnol 2007;1:69–79.
84. Yamada M, Seki M. Hydrodynamic filtration for on-chip particle concentration and classification utilizing microfluidics. Lab Chip 2005;5:1233–1239.
85. Ateya D, Erickson J, Howell P, Hilliard L, Golden J, Ligler F. The good, the bad, and the tiny: A review of microflow cytometry. Anal Bioanal Chem 2008;391:1485–1498.
86. Simonnet C, Groisman A. High-throughput and high-resolution flow cytometry in molded microfluidic devices. Anal Chem 2006;78:5653–5663.
87. Kummrow A, Theisen J, Frankowski M, Tuchscheerer A, Yildirim H, Brattke K, Schmidt M, Neukammer J. Microfluidic structures for flow cytometric analysis of hydrodynamically focussed blood cells fabricated by ultraprecision micromachining. Lab Chip 2009;9:972–981.
88. Hou H-H, Tsai C-H, Fu L-M, Yang R-J. Experimental and numerical investigation into micro-flow cytometer with 3D hydrodynamic focusing effect and micro-weir structure. Electrophoresis 2009;30:2507–2515.
89. Tsai C-H, Hou H-H, Fu L-M. An optimal three-dimensional focusing technique for micro-flow cytometers. Microfluid Nanofluid 2008;5:827–836.
90. Golden JP, Kim JS, Erickson JS, Hilliard LR, Howell PB, Anderson GP, Nasir M, Ligler FS. Multiwavelength microflow cytometer using groove-generated sheath flow. Lab Chip 2009;9:1942–1950.
91. Howell PB Jr, Golden JP, Hilliard LR, Erickson JS, Mott DR, Ligler FS. Two simple and rugged designs for creating microfluidic sheath flow. Lab Chip 2008;8:1097–1103.
92. Choi S, Park J-K. Sheathless hydrophoretic particle focusing in a microchannel with exponentially increasing obstacle arrays. Anal Chem 2008;80:3035–3039.
93. Kim YW, Yoo JY. Three-dimensional focusing of red blood cells in microchannel flows for bio-sensing applications. Biosens Bioelectron 2009;24:3677–3682.
94. Segré G, Silberberg A. Behavior of macroscopic rigid spheres in Poiseuille flow Part 2. Experimental results and interpretation. J Fluid Mech 1962;14:136–157.
95. Chun B, Ladd AJC. Inertial migration of neutrally buoyant particles in a square duct: An investigation of multiple equilibrium positions. Phys Fluids 2006;18:031704.
96. Asmolov ES. The inertial lift on a spherical particle in a plane Poiseuille flow at large channel Reynolds number. J Fluid Mech 1999;381:63–87.
97. Ho BP, Leal LG. Inertial migration of rigid spheres in two-dimensional unidirectional flows. J Fluid Mech 1974;65:365–400.
98. Di Carlo D, Irimia D, Tompkins RG, Toner M. Continuous inertial focusing, ordering, and separation of particles in microchannels. Proc Natl Acad Sci USA 2007;104:18892–18897.
99. Edd JF, Di Carlo D, Humphry KJ, Koster S, Irimia D, Weitz DA, Toner M. Controlled encapsulation of single-cells into monodisperse picolitre drops. Lab Chip 2008;8:1262–1264.
100. Bhagat AAS, Kuntaegowdanahalli SS, Papautsky I. Continuous particle separation in spiral microchannels using dean flows and differential migration. Lab Chip 2008;8:1906–1914.
101. Di Carlo D, Edd JF, Irimia D, Tompkins RG, Toner M. Equilibrium separation and filtration of particles using differential inertial focusing. Anal Chem 2008;80:2204–2211.
102. Mao X, Lin S-CS, Dong C, Huang TJ. Single-layer planar on-chip flow cytometer using microfluidic drifting based three-dimensional (3D) hydrodynamic focusing. Lab Chip 2009;9:1583–1589.
103. Lee MG, Choi S, Park J-K. Three-dimensional hydrodynamic focusing with a single sheath flow in a single-layer microfluidic device. Lab Chip 2009;9:3155–3160.
104. Hur SC, Tse HTK, Carlo DD. Sheathless inertial cell ordering for extreme throughput flow cytometry. Lab Chip 2010;10:274–280.
105. Gossett DR, Carlo DD. Particle focusing mechanisms in curving confined flows. Anal Chem 2009;81:8459–8465.

106. Pamme N. Continuous flow separations in microfluidic devices. Lab Chip 2007;7:1644–1659.
107. Lagally ET, Lee S-H, Soh HT. Integrated microsystem for dielectrophoretic cell concentration and genetic detection. Lab Chip 2005;5:1053–1058.
108. Li Y, Dalton C, Crabtree HJ, Nilsson G, Kaler KVIS. Continuous dielectrophoretic cell separation microfluidic device. Lab Chip 2007;7:239–248.
109. Zhu J, Tzeng T-R, Hu G, Xuan X. DC dielectrophoretic focusing of particles in a serpentine microchannel. Microfluid Nanofluid 2009;7:751–756.
110. Holmes D, Morgan H. Single cell impedance cytometry for identification and counting of CD4 T-cells in human blood using impedance labels. Anal Chem 2010;82:1455–1461.
111. Pierzchalski A, Hebeisen M, Mittag A, Di Berardino M, Tarnok A. Label-free single cell analysis with a chip-based impedance flow cytometer. San Francisco, CA: SPIE; 2010. pp 75681B–11.
112. Steinbrich-Zöllner M, Grün J, Kaiser T, Biesen R, Raba K, Wu P, Thiel A, Rudwaleit M, Sieper J, Burmester G. From transcriptome to cytome: Integrating cytometric profiling, multivariate cluster, and prediction analyses for a phenotypical classification of inflammatory diseases. Cytometry Part A 2008;73A:333–340.
113. Tárnok A, Pierzchalski A, Valet G. Potential of a cytomics top-down strategy for drug discovery. Curr Med Chem 2010 [Epub 26 March, ahead of print].
114. Mittag A, Tárnok A. Basics of standardization and calibration in cytometry: A review. J Biophotonics 2009;2:470–481.
115. Tárnok A, Bocsi J, Pipek M, Osmancik P, Valet G, Schneider P, Hambsch J. Preoperative prediction of postoperative edema and effusion in pediatric cardiac surgery by altered antigen expression patterns on granulocytes and monocytes. Cytometry 2001;46:247–253.
116. Lugli E, Pinti M, Nasi M, Troiano L, Ferraresi R, Mussi C, Salvioli G, Patsekin V, Robinson JP, Durante C. Subject classification obtained by cluster analysis and principal component analysis applied to flow cytometric data. Cytometry Part A 2007;71A:334–344.
117. Valet G. Predictive medicine by cytomics: Potential and challenges. J Biol Regul Homeost Agents 2002;16:164–167.
118. Leif RC, Schwartz S, Rodriguez CM, Pell-Fernandez L, Groves M, Leif SB, Cayer M, Crews H. Two-dimensional impedance studies of BSA buoyant density separated human erythrocytes. Cytometry 1985;6:13–21.
119. Cheung KC, Gawad S, Renaud P.Microfluidic Impedance Spectroscopy Flow Cytometer: Particle Size Calibration. 17th IEEE International Conference on MEMS, Maastricht, 25–29 January, 2004. pp 343–346.
120. Gascoyne PRC, Pethig R, Satayavivad J, Becker FF, Ruchirawat M. Dielectrophoretic detection of changes in erythrocyte membranes following malarial infection. BBA-Biomembranes 1997;1323:240–252.
121. Nascimento EM, Nogueira N, Silva T, Braschler T, Demierre N, Renaud P, Oliva AG. Dielectrophoretic sorting on a microfabricated flow cytometer: Label free separation of Babesia bovis infected erythrocytes. Bioelectrochemistry 2008;73:123–128.
122. Carbonaro A, Mohanty SK, Huang H, Godley LA, Sohn LL. Cell characterization using a protein-functionalized pore. Lab Chip 2008;8:1478–1485.
123. Wang X, Becker FF, Gascoyne PRC. Membrane dielectric changes indicate induced apoptosis in HL-60 cells more sensitively than surface phosphatidylserine expression or DNA fragmentation. Biochim Biophys Acta 2002;1564:412–420.
124. Yang J, Huang Y, Wang X, Wang X-B, Becker FF, Gascoyne PRC. Dielectric properties of human leukocyte subpopulations determined by electrorotation as a cell separation criterion. Biophys J 1999;76:3307–3314.
125. Huang Y, Wang X, Gascoyne P, Becker F. Membrane dielectric responses of human T-lymphocytes following mitogenic stimulation. Biochim Biophys Acta 1999;1417:51–62.
126. Wang X, Huang Y, Gascoyne P, Becker F, Hölzel R, Pethig R. Changes in Friend murine erythroleukaemia cell membranes during induced differentiation determined by electrorotation. Biochim Biophys Acta 1994;1193:330–344.
127. Vykoukal DM, Gascoyne PRC, Vykoukal J. Dielectric characterization of complete mononuclear and polymorphonuclear blood cell subpopulations for label-free discrimination. Integr Biol 2009;1:477–484.
128. Godin J, Chen C-H, Cho SH, Qiao W, Tsai F, Lo Y-H. Microfluidics and photonics for bio-system-on-a-chip: A review of advancements in technology towards a microfluidic flow cytometry chip. J Biophotonics 2008;1:355–376.
129. James CD, Okandan M, Mani SS, Galambos PC, Shul R. Monolithic surface micromachined fluidic devices for dielectrophoretic preconcentration and routing of particles. J Micromech Microeng 2006;10:1909–1918.
130. Holmes D, Sandison ME, Green NG, Morgan H. On-chip high-speed sorting of micron-sized particles for high-throughput analysis. IEE Proc Nanobiotechnol 2005;152:129–135.
131. Baret J-C, Miller OJ, Taly V, Ryckelynck M, El-Harrak A, Frenz L, Rick C, Samuels ML, Hutchison JB, Agresti JJ. Fluorescence-activated droplet sorting (FADS): Efficient microfluidic cell sorting based on enzymatic activity. Lab Chip 2009;9:1850–1858.
132. Shirasaki Y, Tanaka J, Makazu H, Tashiro K, Shoji S, Tsukita S, Funatsu T. On-chip cell sorting system using laser-induced heating of a thermoreversible gelation polymer to control flow. Anal Chem 2005;78:695–701.
133. Sugino H, Ozaki K, Shirasaki Y, Arakawa T, Shoji S, Funatsu T. On-chip microfluidic sorting with fluorescence spectrum detection and multiway separation. Lab Chip 2009;9:1254–1260.
134. Wang MM, Tu E, Raymond DE, Yang JM, Zhang H, Hagen N, Dees B, Mercer EM, Forster AH, Kariv I. Microfluidic sorting of mammalian cells by optical force switching. Nat Biotech 2005;23:83–87.
135. Chen C, Cho SH, Tsai F, Erten A, Lo Y-H. Microfluidic cell sorter with integrated piezoelectric actuator. Biomed Microdev 2009;11:1223–1231.
136. Johansson L, Nikolajeff F, Johansson S, Thorslund S. On-chip fluorescence-activated cell sorting by an integrated miniaturized ultrasonic transducer. Anal Chem 2009;81:5188–5196.
137. Seger U, Gawad S, Johann R, Bertsch A, Renaud P. Cell immersion and cell dipping in microfluidic devices. Lab Chip 2004;4:148–151.
138. Rovera G, Santoli D, Damsky C. Human promyelocytic leukemia cells in culture differentiate into macrophage-like cells when treated with a phorbol diester. Proc Natl Acad Sci USA 1979;76:2779–2783.